Physics – Uspekhi **49** (12) 1263 – 1288 (2006)

INSTRUMENTS AND METHODS OF INVESTIGATION PACS numbers: **07.57. – c**, **87.57. – s**, 87.63.Hg

Modern matrix thermovision in biomedicine †

G R Ivanitsky

DOI: 10.1070/PU2006v049n12ABEH006163

Contents

Abstract. The focal plane array infrared technique (thermovision) is a rapid, noncontact, painless, and harmless diagnostic tool for many diseases. In this paper, the use of remote IR radiation detection to obtain infrared human images and perform spatio-temporal measurements of temperature distribution is reviewed in terms of its historical development. Mechanisms of heat production in the human body, methods to control it, and the effects of environment are briefly discussed. Biomedical applications of matrix thermovision are reviewed.

1. Introduction. Historical review of thermovision

The end of the 20th and the beginning of the 21st centuries has been a period of rapid developments in the entire life sciences sector, with a priority emphasis on genomics, proteomics, cell biology, and bioinformatics. Advances in molecular research gave rise to the avalanche-like process of revision of the available medical facts concerning the predisposition of humans to a variety of diseases, their evolutionary genetics, protective immune mechanisms, and the role of environmental conditions and stress in pathogenesis of many diseases, i.e., factors determining human health, longevity, and ecological well-being. The term *biomedicine* was coined to define the applied aspect of these studies. Matrix thermovision has grown into an information technology for biomedicine.

Some researchers believe that by the year 2025 *biomedical* technologies will eventually transform medicine into a science based on the knowledge of molecular mechanisms underlying the pathogenesis of many disorders and mathematical simulation of diseases for the choice of therapeutic modalities with regard for specific genetic and phenotypic features of individual patients. It is hardly possible to precisely predict further developments in biomedicine from the current rate of scientific progress because time, like a censor, sometimes crosses out and erases exactly what we predict and wish to see realized.

The contribution of physicists to the development of biomedical tools for the diagnosis and management of diseases is illustrated by their participation in the Program 'Fundamental Sciences to Medicine' initiated by the Presidium of the Russian Academy of Sciences. Some problems of mutual interest at the borderline of physics and biomedicine have much in common despite different methods employed by the two sciences for their solution. Thermovision provides a good example of on-going approaches to the search for answers to the questions arising with respect to the development and exploration of these methods.

† This review is an enlarged version of a report presented at the meeting of the Presidium of the Russian Academy of Sciences on 13 December 2005.

G R Ivanitsky Institute of Theoretical and Experimental Biophysics, Russian Academy of Sciences,
ul. Institutskaya 3, 142290 Pushchino, Moscow region, Russian Federation
Tel. (7-0467) 73 24 81. Fax (7-0467) 79 05 53
E-mail: ivanitsky@iteb.ru

Received 30 June 2006, revised 26 September 2006
Uspekhi Fizicheskikh Nauk **176** (12) 1293 – 1320 (2006)
Translated by Yu V Morozov; edited by A Radzig

Why does thermovision find quite limited application in medicine despite its history of more than half a century? What is the mechanism of heat production in living organisms? How is thermal energy generated in the body and what are the implications of its modulation? What new findings can be expected from visualization of different parts of the human body in the infrared (IR) wavelength region? What information can be derived for medical diagnosis from human IR images? What are the requirements for IR radiation detection in humans? How can we chose a thermal imager for biomedical purposes with optimal cost – effectiveness characteristics? These and related problems will be considered in the present review.

A few years ago, the specialized Cabinet of System Biothermography was organized at the Institute of Theoretical and Experimental Biophysics, Russian Academy of Sciences (Pushchino, Moscow region). Joint thermal diagnostic studies were initiated with the I M Sechenov Moscow Medical Academy and Rehabilitation Centre, Department of Management of the President, Russian Federation (Kubinka, Moscow region). Examples of the application of thermovision technologies in these settings are presented in Section 7 of the present communication.

It is long-standing knowledge that the temperature of the human body is an indicator of its physiological state. The first recorded use of human skin temperature for diagnostic purposes can be found in the writings of Hippocrates (around 460 – 377 BC) [1]. In those bygone times, human body temperature was determined by a mere touch. The main emphasis continued to be laid on the development of contact methods for the measurement of body temperature during the long period that followed. A qualitative breakthrough that eventually brought about remote temperature sensing techniques originated in the understanding that infrared emission found in the spectrum of electromagnetic radiation may be related to body temperature. This breakthrough occurred quite recently, in the first quarter of the 20th century [2]. Table 1 shows various stages in the development of temperature measuring techniques for diagnostic purposes in medicine.

Optico-mechanical thermovision systems were born during World War II (1939 – 1945). Most widespread at that time were single-element systems transforming IR radiation into an electrical signal. Optico-mechanical systems were utilized to scan fields of vision. An infrared image was projected point-by-point onto an IR detector – transducer assembly. Electrical signals from the transducer were amplified and transmitted as modulating voltage to a cathode-ray tube. The scanning electron beam was synchronized with the scanning of the IR image field. In this way, the thermal image of the object was formed at the tube screen.

Another qualitative breakthrough occurred 30 years later with the discovery of new chemical structures showing highly variable conductivity at different temperatures or requiring a rather low energy of light quanta for the internal emission of electrons, i.e., suitable for work with IR radiation (e.g., the $HgCdTe_2$ compound). Those substances could be used to sense a relatively long-wave spectral region (wavelengths over 6 μm). Maximum thermal emission from objects placed at room temperature was observed at wavelengths of around 10 μm. Thermal imagers used in the 1970s had a sensitivity of a few fractions of a degree Celsius [3]. Such sensitivity was commensurable with fluctuations of thermal radiation produced by the human body. However, those thermovisors had low spatial resolution and many attempts to widely and effectively use them in medicine resulted in failure. Nevertheless, for all the shortcomings of early thermovision systems, they gradually found an increasingly greater application in various fields of science and technology, including medicine.

When and by whom was thermovision first employed in clinical practice? It is a difficult question to answer. Many consider R N Lawson to be a pioneer in this field since he was the first to apply a night vision camera (previously operated only by military users) for the early diagnosis of breast cancer in women in 1956. Next year, Lawson published a paper entitled "Thermography — a new tool in the investigation of breast lesions" in a Canadian medical journal [4]. Breast thermography proved to be a promising technique. According to Lawson, the reliability of detecting breast cancer, especially at its early stages, was 60 – 70%. Identification of risk groups in large-scale trials was expected to add credence to thermovision as a new method for the express diagnosis of breast cancer.

Table 1. The development of contact and remote temperature sensing methods [2].

Measuring device	Sensitivity of the method, °C	Cost, $	Advent of method	Main advantages	Main drawbacks
Contact measuring methods					
Hand	2 – 3		Before 5st century BC	Ready availability	Subjectiveness
Mercury thermometer	0.1 – 0.2	2	16th century	Low cost, accessibility	Necessity of contact
Thermistors or thermocouples	0.01 – 0.02	2000	1930s	High accuracy, accessibility	Necessity of contact
Thermosensitive films, liquid crystal thermographs	0.3 – 1.0	5000	1960s	Providing thermal imaging	Necessity of contact
Remote measuring methods					
Computerized optico-mechanical thermovision	0.05	75000	1970s	Absence of contact, computer analysis	High cost, low time resolution
Matrix thermovision	0.005	> 100000	1990s	Absence of contact, high accuracy, computer analysis	High cost

It is difficult, however, to confirm the priority of Lawson's thermovision studies because electronic scanning systems for the purpose evolved in parallel with IR equipment for contact measurements without electric transformation and scanning. These devices included thermosensitive films of liquid crystals, luminophors, semiconductors, magnetic materials, and thermosensitive dyes that could be brought in contact with a study object to observe temperature distribution patterns over its surface. This variant of thermovision is also referred to as *thermography*. However, thermography directly measures the temperature of different areas on the object's surface rather than its thermal emission. Thermographic detection is based on the dependence of the film's optical parameters on thermal impact. Such characteristics include light reflection and transmission coefficients or luminescence intensity inherent in a given material. By way of example, certain types of liquid crystals are known to change color when heated. This property allowed their temperature to be visually determined with a high degree of accuracy (to within 0.3 °C).

Interestingly, the very first thermal imagers of this type (even if more legendary than factual) are believed to have been used in ancient Egypt. Doctors of those times spread a mud slurry from the Nile River over their patients and observed which areas changed color first; these were thought to indicate body parts having different temperatures.

Three periods are distinguished in the development of electronic IR cameras for the remote measurement of spatial temperature distribution [5]. First was the period of constructing hybrid electron optico-mechanical systems. Optico-mechanical scanning of an object's image was realized with the help of rotating prisms, Nipkov disks, and swinging mirrors [6]. IR radiation was focused onto a photosensitive cell or an array of such elements and transformed into an electric signal. These devices were replaced by systems consisting of small matrices. Finally, large matrix systems of several thousand IR detectors were created [7 – 12].

Nowadays, two main variants of IR cameras (photonic and microbolometric) are in use, in which two types of matrices are employed. One type in both photonic and microbolometric cameras represents a system of complementary metal oxide semiconductors (CMOS matrices), the other comprises charge-coupled devices (CCD matrices) used in photon cameras. Each variant has its merits and drawbacks. The advantages of CMOS matrices are economic operation and high speed of response — in a static regime, the current is virtually absent and sampling of matrix elements is possible by the snap-shot method. A disadvantage is the high cost of CMOS matrices. CCD matrices suffer another grave shortcoming, which is the readout of information by sequential shift registers transforming a row of input charges into a series of output pulses; this causes noticeable processing slowdowns. The practical use of CCD matrices encounters the very complicated problem of achieving an acceptable dynamic range and sensitivity of the sensor. In recent years, a variety of methods for the rapid readout of information have been proposed. There are improved variants of a full-frame CCD-based system in which parallel register charges do not directly enter a sequential register row-by-row but are first 'stored' in a buffer parallel register and only then transferred to the inlet of a sequential shift register; this improves the operation speed of thermovision systems [13 – 16].

The main results of these developments is the disappearance of optico-mechanical units from all types of modern IR cameras; hence, their smaller dimensions, reduced energy consumption, and, most important, increased signal-to-noise ratio, improved image quality, and broadened dynamic range of the registered signal.

2. The thermal imager as a device for panoramic examination and radiometry

2.1 Design and technical parameters of thermovision devices

There are two potential applications of thermal imagers in medicine, namely, panoramic examination and radiometry, i.e., the remote measurement of absolute temperature at any point on the patient's body. Panoramic examination allows for high-quality visualization in express diagnosis of various diseases. Radiometry enables the user to compare the results of observations throughout large time intervals (the creation of thermal image databases). Modern thermal imagers measure temperature to an accuracy of several fractions of a degree at each 30×30-μm microarea of the object under study. It should be borne in mind, however, that the key word in the term 'thermovision' is '*vision*'. Vision constitutes information process whereby an entire object can be surveyed within a certain IR wavelength range in order to identify and classify it and to reveal its most important attributes. The two wavelength regions most frequently used in thermovision cameras are 3 – 5 and 8 – 12 μm corresponding to two atmospheric transparency windows (see Fig. 1). True, the choice of a spectral range for medical purposes is not dictated by atmosphere transparency alone; the object of interest (a human) being positioned very close to the camera, IR absorption in the air can be neglected [3].

When the IR image of an object is displayed on the monitor screen, conventional variations of the brightness or color of its constituent elements reflect temperature differences between object's surface elements. It should be emphasized that the choice of a coding mode for the temperature representation of an image (color or black-and-white) on the monitor screen is a matter of the operator's taste and experience. An indispensable precondition for IR image formation regardless of the coding modality is a temperature contrast between the object and the background, on the one hand, and among individual elements within the object contour, on the other hand. A result of a panoramic survey is exemplified by Fig. 2, which depicts the IR image of a human taken at two camera angles in the IR radiation

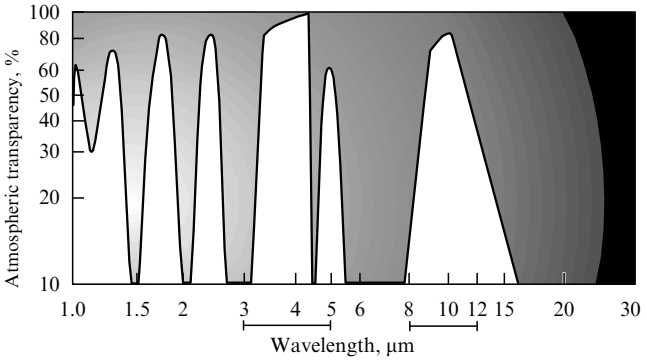

Figure 1. Atmospheric transparency windows for infrared radiation of different wavelengths.

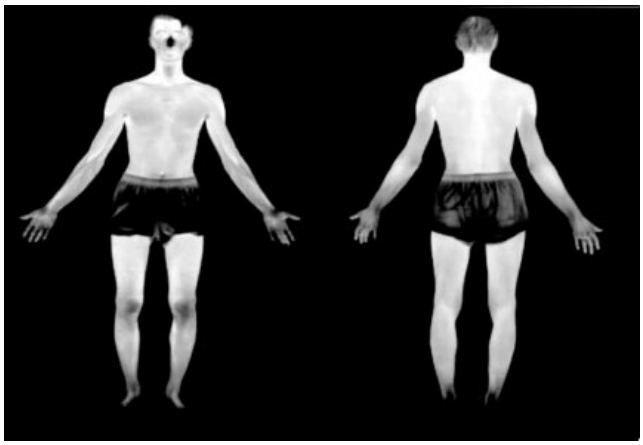

Figure 2. Panoramic human IR image obtained by a microbolometric camera with a matrix of 320 × 240 vanadium oxide elements in an 8 – 12-μm wavelength range.

wavelength range of 8 – 12 μm using a microbolometric camera with a vanadium oxide matrix.

In order to enhance the sensitivity of the measurement and improve the signal-to-noise ratio, matrices consisting of IR photodetectors need to be thermostabilized and cooled. Deep (cryogenic) cooling is achieved using either liquid nitrogen or a gas refrigerator with a closed Split – Stirling cycle that allows for cooling down to an average temperature of ~ 80 K. Moreover, there are systems with a moderate depth of cooling, in which temperatures of 150 – 200 K are obtained. Other cooling methods may also be used for this purpose, such as those using thermoelectric devices based on the Peltier effect. The IR image shown in Fig. 2 was acquired with the use of a not deeply cooled camera.

Photon devices with cooled IR photodetectors are the most sensitive [17] and at the same time the most expensive ones. Their price amounts to several hundred thousand US dollars; much of this sum covers the costs of the cooling systems of the detector and the IR objective.

Figure 3 exemplifies the use of IR radiometry by an image of human fingers with well-apparent open sweat pores measuring approximately 30 μm. Figure 3b demonstrates thermograms of areas *1* and *2* depicted in Fig. 3a. The images were obtained using a deeply cooled photon thermal imager with an indium antimonide matrix.

Matrices for photonic devices are manufactured with the use of heterostructures (such as lead chalcogenide, cadmium – mercury – tellurium compound, indium antimonide, platinum silicide, silicon- or germanium-doped substances); multilayer structures with quantum-well infrared photodetectors (QWIPs), and Schottky barriers of thin (~ 30 Å) platinum silicide films. It can be expected that combinations of such heterostructures within a single sensitive element of a photodetector will be used in the near future [18 – 21]. Vanadium oxide and amorphous silicon are most widely utilized in microbolometers [22, 23].

The main and most attractive sensitivity characteristic of thermal imagers available on the consumer market is noise-equivalent temperature difference (NETD), i.e., noise equivalent of temperature differential. In the promotional materials of manufacturing companies, NETD is sometimes referred to as the limiting thermal sensitivity, although this is not quite correct. In modern thermal imagers with cooled detectors,

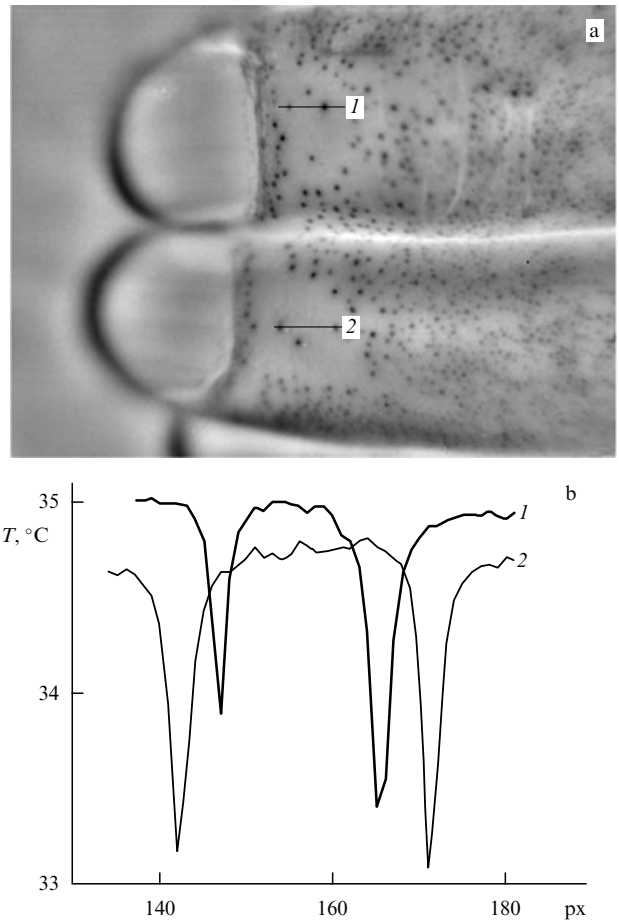

Figure 3. (a) IR image of fingers and temperature measurement of open sweat gland ducts within a wavelength range of 8 –12 μm; spatial resolution reaches 30 μm. Dark points on the fingers are sweat gland ducts. (b) Temperature profile along lines *1* and *2* on the two fingers shown in Fig. 3a. The abscissa is the distance in pixels (px); scale: 1 mm = 8 px.

this parameter varies in a range from 10 to 40 mK. Recent articles on the Internet report NETD values of 5 mK but do not disclose how such sensitivity is achieved. The accuracy of absolute temperature measurement is a rather obscure notion formulated depending on many parameters; commercially available radiometers allow for measurement accuracy falling within 50 – 100 mK.

Another important characteristic is the frequency of information refreshing (frame rate) because dynamic thermometry of different parts of the body using fast Fourier transformation for the analysis makes it possible to assess the state of nervous mechanisms controlling heat production in humans [24 – 26]. The frequency of information refreshment on $HgCdTe_2$ or InSb matrices usually varies from 100 to 400 Hz. It lies in a range of 25 to 100 Hz for devices with IR matrices containing structures of low quantum efficiency, such as Schottky diodes (PtSi/Si).

The users have to resort to various technical tricks in an attempt to broaden the dynamic range of IR radiation intensities detected by thermal imagers and avoid their 'blinding'. Sometimes, this purpose is achieved by the optimal choice of the frame rate or by the charge transfer from the overfilled capacitor of a matrix element to buffer storage units in systems with CCD matrices. Cell capacity of modern CCD matrices is $\sim 10^6 - 10^7$ electrons per matrix element (pixel) depending on manufacturing technology and

Table 2. Predicted demand for thermovision technologies in different spheres of their application.

Area of application	Expected demand, thousands/yr	Fraction of the total, %
Transport equipment • aircraft • ships • trains and motor vehicles	504 2 2 500	40.84
Security and safety systems	500	40.5
Control and diagnostics of various equipment	100	8.1
Aerocosmic monitoring of natural, technogenic, and environmental catastrophes	100	8.1
Energy consumption control in municipal management	20	1.62
Rescue operations	5	0.4
Medical applications	5	0.4
Total	1234	100

operation conditions. However, serious technical difficulties are encountered when the user comes to the prevention of 'blinding' of a device at high object's radiation intensities by increasing the operation frequency. For example, as soon as the matrix format exceeds a currently available value of 2400×1600 elements, the cyclic frequency of electronic equipment becomes the limiting factor because a gigahertz frequency barrier needs to be overcome, which is hardly possible. A radical solution to this problem lies in the development of higher-capacity IR-sensitive matrix elements, e.g., with the capacity in excess of 10^9 electrons per pixel. This is a fundamental challenge for thermal imaging technologies based on the use of CCD matrices.

Thermovision devices with uncooled microbolometric detectors are cheaper. Their minimal cost is some \$20,000. However, the sensitivity of such instruments is almost twice as low as that of cooled photon cameras. Their noise-equivalent temperature difference varies in the range of 40 to 120 mK. Also, they include special systems for thermostabilization of the IR matrix, but as a rule without a cooling agent (liquid nitrogen).

The sensitive elements of microbolometric detectors are characterized by thermal inertia that accounts for their maximum sensitivity being attainable at a matrix refreshing frequency, i.e., below 50 Hz. However, such a frequency is sufficient to resolve most problems facing biomedical diagnosis. One of the factors limiting sensitivity of low-frequency amorphous silicon detectors is a flicker-like noise, the power spectrum of which varies as a function of $1/f$, where f is the signal spectrum frequency. This noise may be responsible for the distortion of the object's temperature profile fronts and for the impaired resolving power of the camera. Commercially available uncooled detectors calibrated as radiometers measure absolute temperatures in the range of human physiological functions to within 0.04 °C.

2.2 Demand for thermal imagers in medicine

A detailed description of the construction of matrix thermal imagers and their modifications is beyond the scope of this review. The interested reader is referred to promotional booklets of the respective manufacturing companies and scientific publications [7–22]. Suffice it to say that over 20 companies in the USA, France, China, Israel, Russia, and other countries presently offer and market matrix thermovision devices.

Software of a modern thermovision camera allows for online digital processing of an IR image, calculating thermal profile parameters, and creating a computerized database of IR images and comparing those obtained at different times. The electronic journal *ESKO* published by the energy service company Ecological Systems forecasts (No. 2, February 2004) further expansion of the already wide world market for thermovision devices and projects a rise in its annual value to almost 200 billion US dollars. However, purchases of the thermal imagers for medical purposes are not expected to exceed 0.4% of the total (Table 2).

There are several reasons for a relatively small number of thermal imagers currently in use in medicine. The main one is the poor understanding of the tremendous and sometimes unique opportunities opened up by thermal imaging technologies for the study of human vital activities. Another reason is the relatively high cost of this equipment.

Areas on the human body with anomalously high or low temperatures may be indicators of underlying organ pathology even at the early stages of its development (the literature cites 150 diseases diagnosed by the methods under consideration [27]).

Many clinicians with whom we happened to co-operate believe that thermal imagers cooled by liquefied gas are too costly and inconvenient to use, especially in the operating room. Personnel of small hospitals are reluctant to work with containers of liquid nitrogen and bear additional expenses for their purchase and transportation. What they actually need are small and easy to operate microbolometric cameras requiring no liquid nitrogen for cooling [17, 23]. However, such cameras have drawbacks, such as low temperature sensitivity and a narrower range of ambient temperatures within which results of thermometry may be considered reliable. For these reasons, such devices do not find wide application in biomedical research.

3. Humans as the objects of thermodynamic studies

3.1 Ways in which and in what amounts humans receive heat

It is necessary to consider, even if in brief, physical mechanisms of heat production in order to understand what information about the physiological state of the body can be

derived from the observation of spatio – temporal IR images of the human body surface.

When raising the room temperature, it is impossible in principle to have the human body temperature equal to the ambient one. Humans constitute a nonequilibrium thermodynamic system, the work of which is directed, inter alia, towards the maintenance of constant internal body temperature.

The energy of any process never disappears but undergoes transformation from one form to another. It is eventually converted into heat and can no longer be used to do work after the temperature is uniformly distributed throughout the bulk tissue. *However, like any living organism, humans are an open system, the functioning of which depends on the inflow and outflow of substance and energy. Energy is never completely depreciated as it is converted into heat while an organism is alive.* It is easy to see from the isotherms on the surface of the human body, shown in Fig. 4, that its different parts always have different temperatures. It is hardly possible to evaluate the efficiency of humans as 'heat machines' because it is different when we are at rest and in the active state. In the end, we receive all available energy from the Sun. The amount of energy necessary for an individual depends on his or her power inputs, as well as on age and gender [28]. Table 3 illustrates averaged percent distribution of the energy obtained by a person with ingested food [29, 30].

It is immaterial for the assessment of human heat production whether a person feeds on fruits or animal products. The amount of energy per unit time necessary to maintain basal metabolism in humans equals 1600 – 1700 kcal day^{-1} or 70 kcal h^{-1}. It increases to 5000 kcal day^{-1} during active work and may be even higher than 500 kcal h^{-1} when running or lifting weights. The mean muscular energy in a human being is around 150 W, an equivalent to 127.5 kcal h^{-1}. The average heat production in a person of active age is 370 kcal h^{-1} [30].

The cells of the body are its fuel elements. They make up a heating system spread throughout the entire body. A cell uses two types of fuel to generate thermal energy. The first one, in order but not in importance, is fat that undergoes oxidation, yielding approximately 10% of the total heat produced in the human body. The second and main source is oxidation of carbohydrates, for example, glucose, accounting for 90% of the energy converted in the body. It is not difficult to evaluate the energy produced in either process [31]. A living cell, regardless of it localization in the body, is home to three types of reactions, namely, free oxidation unrelated to biosynthesis of ATP (adenosine triphosphate) molecules, oxidation coupled to energy accumulation (ATP synthesis), and ATP hydrolysis with transformation to ADP (adenosine diphosphate). The first reaction, i.e., oxidation of lipids, can be written in the general form as

$$XH_2 + PH + O_2 \rightarrow X + POH + H_2O\,, \qquad (1)$$

where XH_2 is the natural donor of hydrogen proton, PH is the substrate undergoing hydroxylation, and POH is the product-hydroxyl of the substrate. In the body, the concentration of XH_2 substances involved in reaction (1) is usually much lower than that of glucose. The integrated heat production is easy to evaluate by directly measuring a decrease in oxygen in the exhaled air. The amount of oxygen involved in lipid oxidation is relatively small. Under normal conditions, only 10% of the oxygen being consumed is needed to maintain free oxidation of lipids, whereas the bulk of it is utilized for the synthesis and splitting of ATP. The exceptions are inflammatory processes and adaptation to cold, i.e., to temperatures below 267 K.

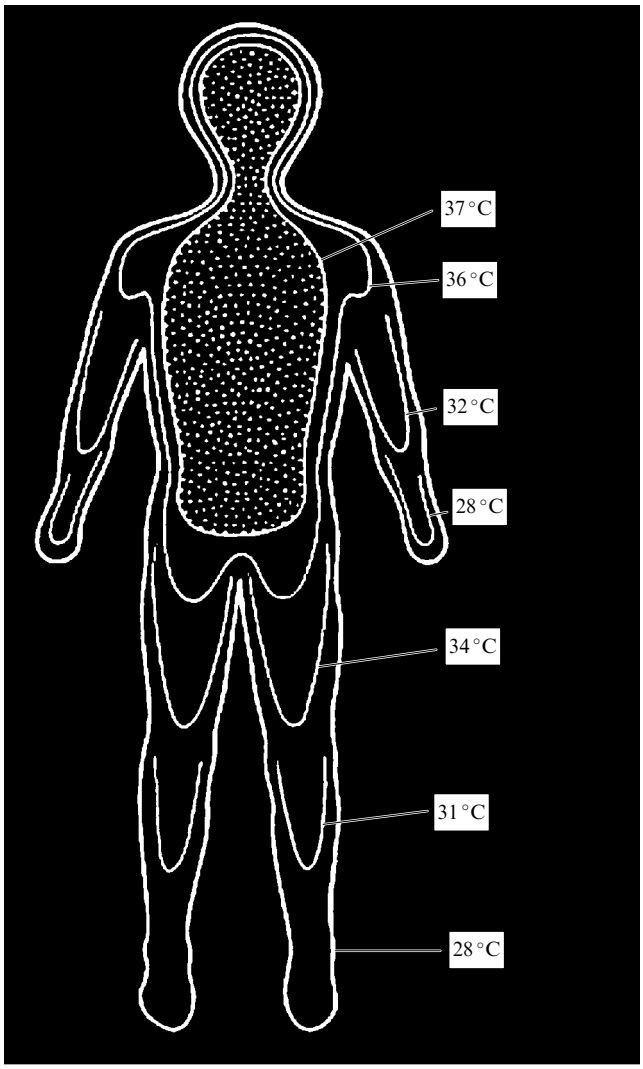

Figure 4. Isotherms on the human body surface.

Table 3. Distribution of energy obtained by ingesting food.

Energy extracted from food	100 %
Loss in $T\Delta S$ (where ΔS is increment of entropy)	5 %
Biochemical loss	50 %
Loss in metabolic cycles	45 – 20 %
Loss during mechanical work (contraction of skeletal muscles)	0 – 25 %

Note. Aerobic combustion: 1 mole of glucose releases 686 kcal of heat. Controlled biological oxidation: 1 mole of glucose produces 38 moles of ATP ($\approx$ 340 kcal of free energy).

Reactions of the second type (biosynthesis of ATP) are localized to cell mitochondria. Glucose oxidation during glycolysis and the Krebs cycle resulting in the production of ATP from ADP can be represented in the following general form [31, 32]:

$$C_6H_{12}O_6 + 38(ADP + P_{in}) + 6O_2 \rightarrow 6CO_2 + 38\,ATP + 44H_2O\,, \qquad (2)$$

where $C_6H_{12}O_6$ is glucose, and P_{in} is inorganic phosphate.

More than half of the energy released from the living cell as a result of oxidation is stored in the form of phosphate bonds. When the reaction is conducted in a tube, 10 kcal of energy is spent to produce one gram-molecule of ATP. Consumption of energy in a living cell is somewhat smaller (7–8 kcal) owing to the presence of enzyme systems. The thermodynamic efficiency of energy extraction by the cell during glucose oxidation is possible to calculate from the total yield of ATP. The initial splitting of glucose into two molecules of lactic acid leads to the production of two ATP molecules and ensures the transfer of six pairs of electrons through the respiratory chain. Each electron pair contributes to the conversion of three ADP molecules into ATP. In other words, decomposition of 1 gram-molecule of glucose in the free respiration process produces 38 gram-molecules of ATP that may give, in the limit, 340–380 kcal of energy from a total of 689 kcal contained in the initial gram-molecule of glucose. *This means that the maximum efficiency of the conjugation between glycolysis and respiration processes* (*in the Krebs cycle*) *may be considered equal to 55%*.

It follows from expression (2) describing a stationary state that synthesis of 38 gram-molecules of ATP requires that 1 gram-molecule of glucose be 'burned' together with 6 gram-molecules of oxygen. This means that ATP synthesis is maintained when oxygen molecules enter a cell at a rate 6 times that of glucose. Part of the energy produced during glucose catabolism (45%) is directly converted into heat, comprising 310 kcal per 1 gram-molecule of glucose [33]. The remaining 55% of energy is stored in energy-rich bonds of ATP and thereafter utilized by the cell to support its vital activities, including energy supply of biosynthetic processes, maintenance of osmotic pressure, active transport, and mechanical and electric work. Consumption of this energy is described by the reaction of the third type (ATP hydrolysis with transformation to ADP) that can be written in the general form as

$$S_i + ATP \rightarrow P_i + ADP + P_{in}\,. \qquad (3)$$

Here, substrate S_i passes during ATP hydrolysis into a new molecular state — product P_i, ADP, and inorganic phosphate P_{in}. The exact efficiency of this process, e.g., during mechanical muscular work, is difficult to estimate. The literature contains contradictory reports. For example, Ref. [34] indicates that the amount of heat liberated during and after muscular contraction is greater than that at rest and depends on the degree of muscle shortening. It may be roughly estimated that heat release averages 5×10^{-3} cal per 1 gram of muscular mass. In other words, 266 kcal of the 380 kcal of energy expanded in ATP during its synthesis is converted into heat. Hence, the efficiency of a muscular cell is on the order of 30%. This means that 70% of the muscle cell energy is directly converted into heat and the remaining 30% turns into heat during muscular work.

Summation of the energy converted into heat in type 2 and 3 reactions gives 576 kcal per 1 gram-molecule of glucose. The efficiency of the cyclic system in the ADP → ATP → ADP chain amounts to $[(689-576)\,100\%]/689 = 16.4\%$; the remaining 83.6% of energy directly transfers into heat, while extra ATP is 'reserved for storage', to be utilized and converted into heat as appropriate in the course of further mechanical, chemical, osmotic, and electric work on mass transport in the body. In the absence of a glucose deficit, as much as 576 kcal is converted into heat per 6 gram-molecules of O_2. Thus, the efficiency of a human as a 'heat machine' may be roughly estimated at 15–20%, the consumption of O_2 and production of CO_2 being its main indicators. Direct measurement of these parameters provides important supplementary information for diagnostic interpretation of human IR images.

3.2 Control system of heat production in the human body

From engineering practice in constructing heating devices come three well-known modes of thermoregulation, namely, variation of heat-exchange surfaces, application of circulating cooling agents (liquids and gases), and regulation of thermal regimes by varying the heating intensity of fuel elements themselves. The same three modalities operate in the human body.

However, humans are not the crown of evolution in terms of heat production control because the efficiency of their 'heat machines' is inferior to that of some other warm-blooded animals, such as winter-dormant mammals. These animals much more efficaciously adapt themselves to variations in ambient temperature by regulating cellular metabolism in a very broad range and thus lowering heating intensity in their bodies [35].

It was found as long ago as the late 19th century that the body temperature of large mammals is lower than smaller ones. At the same time, it was shown that their energy consumption per 1 g of body weight is roughly equal, amounting to about 200 kcal (840 J kg^{-1}) [36, 37]. The reason seemed quite understandable because the source of heating is known to be metabolic processes in individual cells and the number of cells is proportional to the body volume (weight). However, heat elimination from the body surface proves as important as heat production [37]. As a general rule, the more the animal weight, the smaller the surface-to-volume ratio. Moreover, the distributed cellular heating system turns out to be supplemented by central heat control mechanisms governed by the brain and highly specific in different species [38].

A modern concept of thermal regulation in humans is illustrated by the diagram constructed in Fig. 5. Heat and cold receptors generate input ambient temperature signals and the brain (first and foremost, the hypothalamus) 'makes a decision' to release heat in the case of overheating or enhance its production in overcooling.

Blood and the cardiovascular system play an important role in the mechanism of heat distribution throughout the body. On the one hand, five or six litres of blood circulating in the ramified vascular network (Fig. 6) bring with it an oxidizer (oxygen) to each cell of the tissue and thus maintain heat evolution. On the other hand, blood plasma (water) cools organs as it passes through them. These processes are regulated by constriction and dilation of blood vessels and by heart rate modulation. Blood circulation helps to keep internal body temperature at a practically constant level (the 'physiological norm' being around 37 °C). Because the work of individual organs differs in terms of intensity, the mean blood volume passing through each of them per unit time is also different. Table 4 collates blood volumes flowing through various human organs for 1 minute.

The quantity of oxygen extracted from blood by cells is an organ-specific variable. Cells of *resting* skeletal muscles consume little oxygen (only 1.6–2.4 μl per 1 g of tissue per minute) and therefore produce little heat. Oxygen consumption expressed in the same units is 19–33 in the liver, 35 in the

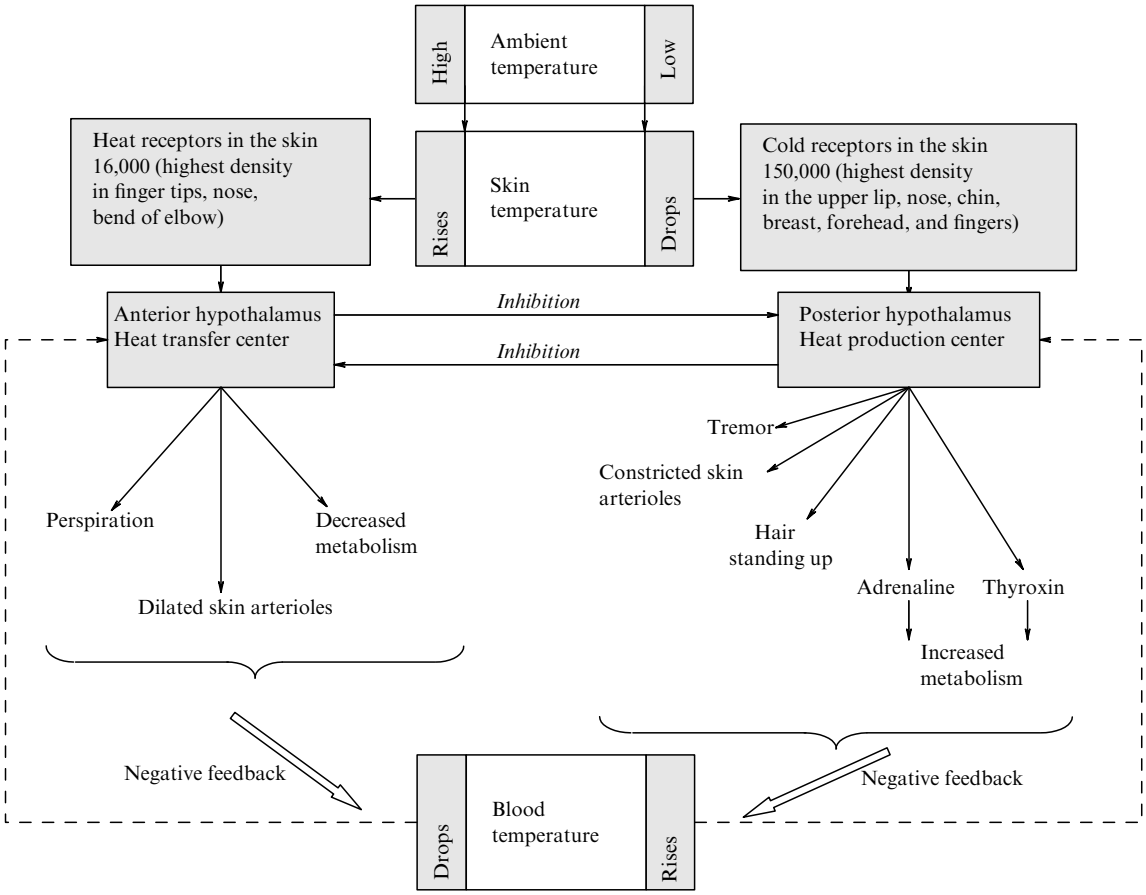

Figure 5. Schematic of thermal regulation in the human body.

brain, 50 – 60 in the kidneys, and 70 – 100 in the heart (at rest) [30]. This means that the cardiac muscle at rest consumes the most energy per unit weight. At the same time, somatic muscles may become the main energy-consuming organ in a person performing hard physical work.

Oxygen transport to organ tissue is realized first and foremost through the capillary blood circulation (microcirculation) system. The total volume V_{O_2} of oxygen consumed by an organism per minute can be expressed as [39]

$$V_{O_2} = q\, C_{(a-v)}, \tag{4}$$

where q is the cardiac output [l min^{-1}], and $C_{(a-v)}$ is the difference between oxygen concentrations in arterial and venous blood [g l^{-1}]. In a person weighing ≈ 70 kg, the cardiac output at rest is $q \approx 4.5-5$ l min^{-1}. However, it varies in a broad range and may be as high as 30 l min^{-1} during intense physical activity. One complete cycle of blood circulation (5 – 6 l) in a healthy human body at rest takes 1 minute. Only about 5.2 g of the total hemoglobin present in each litre of blood is involved in oxygen transport. Nevertheless, a two-fold drop in the hemoglobin level (to 2.6 g l^{-1}) may be fatal since it cannot be compensated for by an increase in cardiac output. In such cases, administration of gas-transporting blood substitutes [40], such as *perftoran* [41], is needed.

Only 10 – 15% of total blood oxygen is utilized at rest. The amount is regulated by the ability of peripheral capillaries to close. The closure is triggered by signals coming from the brain. In elderly persons, pathological capillary spasms may occur spontaneously. A permanently low temperature of the hands and feet in young persons indicates an underlying pathology (e.g., Raynaud's disease, see Fig. 7), whereas in older people it may reflect the decreased diameter of blood vessels as a result of cholesterol deposition on their walls or disturbed nervous regulation (see Section 7.4). A capillary spasm prevents filling microvessels with blood and oxygen delivery to the respective tissue. The most efficient way to overcome oxygen deficit (tissue ischemia) is medicamentous or surgical (including vascular reconstruction) treatment for restoration of normal blood microcirculation.

The total blood volume in the arterial (V_a), venous (V_v), and capillary (V_c) systems, for example, in a 30-year-old 1.76-cm-tall man weighing 70 kg, is $V_a = 1.5$ l, $V_v = 3$ l, and $V_c = 0.5-0.33$ l, respectively. In other words, the microvascular system contains 8 – 10% of all blood present in the human body. The number of capillary vessels in a human amounts to 7×10^{10}, and blood volume in one capillary is 5×10^{-9} cm^3 [31]. The volume V_{O_2} of oxygen transported by blood in capillaries of equal length is a function of their diameter x [42]:

$$V_{O_2} = V_{O_2\,max}\left(1 - \frac{x_{max} - x}{x_{max}}\right), \tag{5}$$

where $V_{O_2\,max}$ is the maximum oxygen volume transported through capillaries, and x_{max} and x are the maximum and actual capillary diameters, respectively. The opening of capillary vessels strongly depends on the synthesis of nitrogen oxide (NO) in tissue cells. Nitrogen oxide relaxes

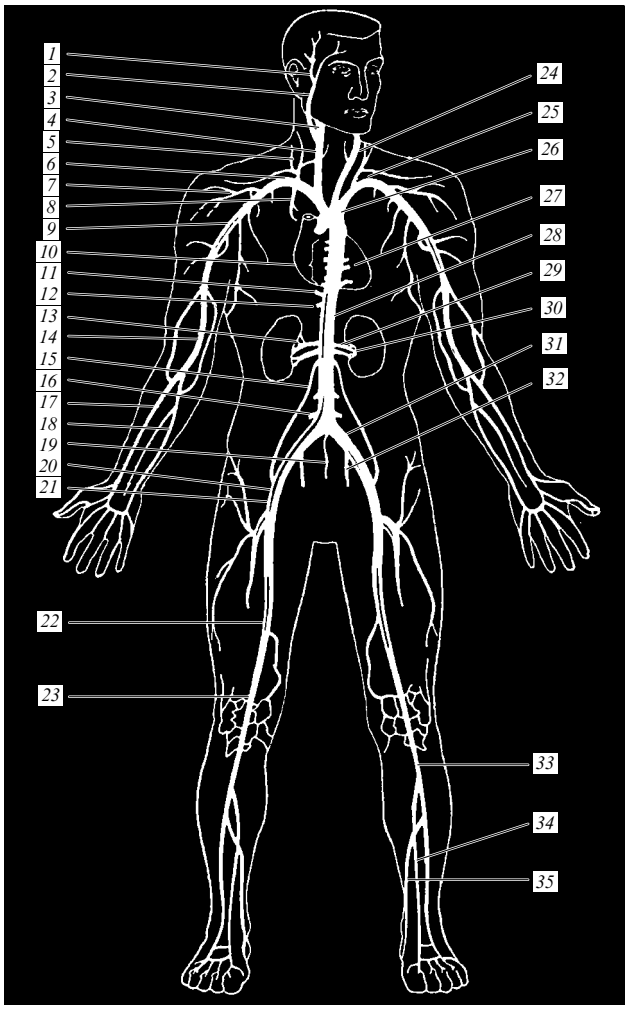

Figure 6. Schematic representation of the human arterial system (venous system is not shown): *1* — superficial temporal, *2* — external carotid, *3* — internal carotid, *4* — cephalic, *5* — costocervical trunk, *6* — thyrocervical trunk, *7* — left subclavian, *8* — internal mammary, *9* — axillary, *10* — intercostal, *11* — superior phrenic, *12* — inferior phrenic, *13*— superior mesenteric, *14* — brachial, *15* — spermatic, *16* — inferior mesenteric, *17* — radial, *18* — ulnar, *19* — median sacral, *20* — external iliac, *21* — femoral, *22* — femoral, *23* — popliteal, *24* — vertebral, *25* — right subclavian, *26* — innominate (brachiocephalic trunk), *27* — esophagal, *28* — celiac, *29* — middle suprarenal, *30* — renal, *31* — common iliac, *32* — internal iliac, *33* — anterior tibial, *34* — fibular, and *35* — posterior tibial.

Table 4. Distribution of blood volume from the left ventricle of the heart over human organs at rest [30].

Organ	Organ weight, kg	Blood flux		Resistance*
		ml min^{-1}	ml $(100\ g\ min)^{-1}$	
Hepatic portal system	2.6	1500	57.7	1.56
Kidneys	0.3	1260	420.0	0.214
Brain	1.4	750	53.6	1.67
Skin	3.6	462	12.8	7
Somatic muscles	31	840	2.7	33.3
Cardiac muscles	0.3	252	84	1
Remaining tissues	23.8	336	1.4	64.3
Whole body	63	5400	8.6	10.6

* Resistance is the ratio of average arterial pressure in mm Hg to the blood flux in ml per 100 g of tissue for 1 min.

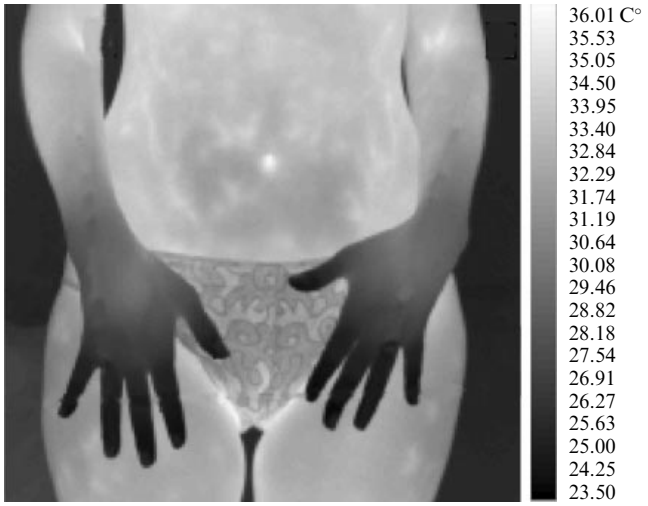

Figure 7. Panoramic IR image of a 23-year-old woman with Raynaud's disease (acute microcirculatory disturbance in hand extremities).

smooth muscles in capillary walls, opens the capillary lumen, and stimulates local production of heat due to O_2 inflow into tissue cells. Synthesis of nitrogen oxide, in turn, depends on oxygen supply.

The system of cardiovascular control in healthy humans effectively maintains internal body temperature at a constant level against a relatively wide range of ambient temperature variations: from −6.7 °C to 32 °C in the air, and from 26 °C to 32 °C in water. The humoral system (thyroid gland) also essentially contributes to the formation of the 'human thermal image' [43].

A number of specific functions of thermoregulation systems responsible for human adaptation to environmental conditions await clarification of their dependence on genetic factors and modification during the course of acclimation. The acquired changes are not inherited. Thermovision technologies may substantially promote relevant research by providing new data on the temperature distribution topography over the human body. It is already known that heat production in the Inuits may increase substantially compared with that in the residents of southern regions [by 22 kcal $(m^2\ h)^{-1}$] from a baseline level of 55 kcal $(m^2\ h)^{-1}$ in an ambient air temperature of 17 °C. In contrast, heat production in indigenous African people is reduced to a minimum and the functioning of their cooling system, e.g., opening of sweat pores, is subject to marked variations, while skin temperature undergoes marked diurnal and seasonal fluctuations. The white race has a mixed-type thermoregulation system [38].

Diurnal and seasonal fluctuations in mean internal temperature of the human body are in the range of 0.1–0.6 °C (it is minimal on summer nights, and maximal in the afternoon in winter). Ovulation in women is accompanied by a 0.6–0.8 °C rise in body temperature on the average. Also, it is known that the integrated temperature of the left side of the human body is higher than that of the right side in 54% of subjects, probably due to the asymmetric anatomic location of the heart.

The brain controls internal body temperature not only by variation of the vascular system carrying capacity and the rate of blood flow but also by the adjustment of the lung surface and breathing rate and intensity to enable support for

Table 5. Parameters influencing the human thermal image.

Parameter	Value
Parameters influencing heat production in the body	
Consumption of O_2	250 ml min^{-1} (respiratory quotient 0.8)
Breathing capacity	4.2 l
Blood volume (plasma + regular blood elements)	5.0 l
Minute cardiac volume	5 l min^{-1} (at rest) or $3.0 + 8M$ [l min^{-1}], where M is O_2 consumption
Mean circulating platelet	0.43
Arterial pressure	120 mm Hg/80 mm Hg
Heart rate (pulse)	65 beats/min
Release of CO_2	200 ml min^{-1}
Total fat content (15% of body weight)	10.2 kg
Energy conversion rate	72 kcal h^{-1} or 40 kcal m^{-2} h^{-1}
Parameters influencing heat release from the body	
Body surface area	1.9 m^2
Lung surface	90 m^2
Total lung volume	6.0 l
Breathing volume	0.5 l
Dead space volume in lungs	0.150 l
Total fluid volume including	51 l (75 %)
Intracellular fluid	27.2 l (40 %)
Tissue fluid and lymph	20.4 l (30 %)
Plasma	3.4 l (5 %)
Subcutaneous fat thickness	5 mm
Height	1.76 m
Weight	70 kg

additional cooling in case of overheating. In humans, the lung surface is 50 times the total body surface.

Table 5 summarizes the main physiological parameters influencing the human thermal image [30]. Almost all of them are amenable to direct measurement. Knowledge of these parameters is essential for the correct interpretation of human IR images aimed at establishing a clinical diagnosis. The data in Table 5 hold for a concrete healthy person of active age. When applied to other people, they give an idea of the relationship between the normal vital characteristics of a human being.

4. Effect of environment conditions on the human thermal image and requirements for infrared radiometric procedure

4.1 Heat balance on the human body surface

In order to exclude artifacts in biomedical diagnosis, it is necessary to take into consideration in the analysis of IR images of the human body environmental conditions that may be responsible for appreciable changes in skin temperature and the thermal topography of the body surface.

Everyone knows from his or her life experience that a person entering a warm room from the cold outside has a lower skin temperature of the exposed body parts than the people who had been in the same room for a longer time. In order to feel comfortable in hot apartments, we switch on an electric fan to set the air in motion and thereby decrease skin temperature. We sweat on a hot sunny day and this saves us from overheating. Skin temperature drops in cold weather. Cold makes us shiver and shivering warms the body.

When any environmental parameter (pressure, humidity, or temperature) is measured near a human body, the result is influenced by the heat produced in the body. Vice versa, all magnitudes of human heat production measured on the skin surface depend on ambient factors.

Based on the first thermodynamic law, heat balance for the human skin surface may be represented in the standard form as [44]

$$M - W = C + E + R\,, \tag{6}$$

where the left-hand side contains energy transferred to the skin surface, and the right-hand side shows quantities of heat energy liberated into the environment: M is metabolic energy generated inside the body (its values were presented in Section 3.1), W is the energy loss owing to mechanical work done by organism, C is heat loss due to air convection, E is the energy lost with water evaporated from the body surface, and R is the energy loss through heat radiation from the skin surface. At rest, the heat losses resulting from somatic muscle activity are vanishingly small but W is not zero because internal organs (heart, gastro-intestinal tract, etc.) never completely cease doing mechanical work.

Radiation loss R recorded by a thermal imager is the sum of two quantities. One is the loss of radiation as a result of interaction between the body having temperature T_0 and the air of temperature T_a. This interaction can be described with the use of the Stefan – Boltzmann constant σ on the assumption that both the air and the body emit energy; in this case, the net loss is given by

$$\sigma\,(T_0^4 - T_a^4) = h_R(T_0 - T_a)\,, \tag{7}$$

where h_R is the radiation transfer coefficient. The exact estimate of h_R corresponds to $4\sigma\bar{T}^3$, where $\bar{T}$ is the intermediate temperature between T_0 and T_a, close to the average one. In practice, h_R can be estimated rather accurately by choosing one temperature, either T_0 or T_a, instead of $\bar{T}$ or by the procedure described in Ref. [45].

The second term defines the additional radiation energy emitted by an external heat source, for example, the Sun or a lamp bulb. This component is frequently referred to as an *effective radiant flux* (following Gagge [46]) or isothermal net radiation R_{ni} (as proposed by Monteith [47]). The quantity R_{ni} is the radiation energy absorbed by the body surface in addition to the energy emitted by the air at a given temperature [47]. The resulting total radiation lost by the body is defined as

$$R = h_R(T_0 - T_a) - R_{ni}\,. \tag{8}$$

The energy loss through air convection at high body temperature may be described as

$$C = h_C(T_0 - T_a)\,, \tag{9}$$

where h_C is the coefficient of heat transmission due to air convection. Taking into consideration Eqns (8) and (9), one finds

$$C + R = h_{CR}(T_0 - T_a) - R_{ni}\,, \tag{10}$$

where $h_{CR} = h_C + h_R$ is the integrated coefficient of temperature loss due to air convection and heat emission.

4.2 Body temperature variations during perspiration

The human body contains from 45 to 75% water by weight, depending mainly on fat deposits. Water content in a given subject changes with age. The blood plasma water occupies minimal volume, while maximum volume is occupied by extracellular fluid (see Table 5). Moreover, part of body water, like CO_2, is synthesized as a final product of lipid and glucose oxidation that simultaneously generates heat energy [see expressions (1) and (2)].

We lose moisture due to evaporation of water through the skin even in the absence of marked perspiration (*ca.* 500 ml of water in 24 hours on average). A rise in ambient temperature causes us to sweat, first by activation of progressively more sweat glands and thereafter (when all of them are involved in the process) by increasing their productivity. By way of example, as much as 2 l of sweat may be discharged in 1 hour at an air temperature above 50 °C.

The second term describing this process on the right-hand side of expression (6) is the latent energy loss by the body with a high temperature through water evaporation from its surface (sweating). This loss of energy can be described in the analytical form as

$$E = h_{\mathrm{E}} \frac{e_0 - e_{\mathrm{a}}}{\gamma} , \tag{11}$$

where e_0 is the mean vapor pressure at the skin surface, and e_{a} is the vapor pressure in the surrounding air [47]. A correction factor is needed because the partial pressure fraction of the total aqueous vapor, produced by water evaporation from the skin surface, is significantly greater than the atmospheric pressure [48]; in practice, however, the emerging error is frequently smaller than the measurement error.

Parameter γ (the so-called *psychrometric index*) is introduced to have coefficient h_{E} equidimensional with h_{C}, i.e., [W m^{-2} °C^{-1}]. At a temperature of 20 °C and standard pressure value of 1013 mbar, $\gamma = 0.66$ mbar °C^{-1}. Quantity e/γ has a temperature dimension and plays the same role as temperature potential in the equation for the latent energy transfer due to air convection from a body with high temperature to the low-temperature environment.

For the special case of $h_{\mathrm{E}} = h_{\mathrm{C}} = h$, Eqns (9) and (11) may be written as the sum of heat loss through convection and energy loss via cutaneous evaporation:

$$C + E = h(\theta_0 - \theta_{\mathrm{e}}) , \tag{12}$$

with $\theta = T + e/\gamma$.

The quantity θ is termed *equivalent temperature*. In fact, three equivalent temperatures are distinguished, denoted by θ_0^*, θ_{e}^*, and θ_{a}^*. The first temperature θ_0^* is directly related to the human body, the second, θ_{e}^*, is environmental temperature (as indicated by the subscript 'e') or the air temperature far from the body, and the third, θ_{a}^*, is determined by the air pressure, humidity, and temperature close to the body surface, i.e., the skin. For every equivalent temperature there are specific e and γ values. All θ_0^*, θ_{e}^*, and θ_{a}^* quantities have a temperature dimension. Their analytical expressions will be presented in Section 4.3 [see formulas (14)–(18)].

The human body cannot reach the air temperature before all the water it contains has evaporated. However, complete dehydration is fatal for a human. Therefore, anyone alive has a wet body temperature (called 'humid temperature' for shortness) to which a temperature increment is added; the increment can be diminished by water evaporation from the wet body. These two temperatures are related by the equation

$$\theta_0 = T' + \frac{e_{\mathrm{w}}(T')}{\gamma} , \tag{13}$$

where $e_{\mathrm{w}}(T')$ is saturated vapor pressure at temperature T'.

4.3 Integrated heat loss in humans

Equations (10) and (11) give the expression for the right-hand side of Eqn (6):

$$C + R + E = h_{\mathrm{CR}}(T_0 - T_{\mathrm{a}}) + \frac{h_{\mathrm{E}}(e_0 - e_{\mathrm{a}})}{\gamma} - R_{\mathrm{ni}} . \tag{14}$$

The equivalent temperature θ^* may be defined as

$$\theta^* = T + \frac{e}{\gamma^*} , \tag{15}$$

where γ^* is the altered form of the psychrometric constant: $\gamma^* = \gamma h_{\mathrm{CR}}/h_{\mathrm{E}}$. Substitution of the appropriately modified psychrometric constants into Eqn (4) leads to

$$C + R + E = h_{\mathrm{CR}}(\theta_0^* - \theta_{\mathrm{a}}^*) - R_{\mathrm{ni}} . \tag{16}$$

The final step in this consideration is the introduction of an increment from external heat radiation increasing the air temperature. It permits taking into account the influence of the external source of radiation energy [46]. The increment may be defined as

$$\theta_{\mathrm{e}}^* - \theta_{\mathrm{a}}^* = \frac{R_{\mathrm{ni}}}{h_{\mathrm{CR}}} , \tag{17}$$

where θ_{e}^* is the equivalent ambient temperature, and θ_{a}^* is the equivalent air temperature in the immediate proximity to human body. Hence, the left-hand side of heat balance equation (6) may be written in the form

$$M - W = h_{\mathrm{CR}}(\theta_0^* - \theta_{\mathrm{a}}^*) , \tag{18}$$

where $M - W$ is the net metabolic energy responsible for high body temperature, expressed as the product of the transfer coefficient h_{CR} and the difference $\theta_0^* - \theta_{\mathrm{a}}^*$ between equivalent temperatures of the body and the air. The state of the environment, including relevant values of air temperature (as well as air humidity, velocity of motion, and IR radiation) is characterized by the parameters h_{CR} and θ_{a}^*. The human skin temperature is given by θ_0^*. Moreover, quantities h_{CR} and h_{E} depend on the body shape and size, while θ_0^* is a function of the air velocity (wind) and body moisture taken into account in the parameter γ^*.

To summarize, the quantity $M - W$ is the total high temperature produced per unit area of the body surface. External environmental factors being constant, there is a range of air temperatures usually called the *thermoneutral zone* within which $M - W$ takes a minimal value regardless of the air temperature. It is desirable to work in the thermoneutral zone to be able to compare the results of measurements taken by thermovision devices.

Equation (18) makes it possible to define the thermoneutral zone as a regime in which $M - W$ assumes a minimal value independent of the real equivalent ambient temperature θ_{e}^*. Any increment of θ_{e}^* in the bounds of this zone is correlated with an equal change in θ_0^* in the same direction;

therefore, the difference $\theta_0^* - \theta_a^*$ is constant. The minimal θ_0^* value and constancy of difference $\theta_0^* - \theta_a^*$ within the thermoneutral zone are actually determined by heat production control inside the human body (see Section 3.2). It should be recalled that h_{CR} is the integrated coefficient of high temperature transfer during convection and heat emission, viz. $h_{CR} = h_C + h_R$. The quantity h_R is given by $4\sigma T^3$, where T is the corresponding average temperature; for example, at $T = 25\,^\circ$C, one obtains

$$h_R = 6.0\ \mathrm{W\,m^{-2}\,s^{-1}}\ . \tag{19}$$

The value of h_C depends on the shape and size of the body, specifying its cooling in the air convection regime. Under forced convection conditions, the transfer coefficient for a subject placed in an air stream flowing around it with a uniform velocity is a function of the wind velocity and the body surface area [44]. *In the same conditions, the transfer coefficient in a person staying upright is approximately 15–20% higher than in a supine position. Deviation from the average value may reach* $\pm 10\%$, while

$$h_C = 7.6\, v^{0.5}\,, \tag{20}$$

where v is the average wind velocity in [m s^{-1}], and the dimensionality of h_C is in [W m^{-2} s^{-1}]. The velocity v at a certain height, e.g., 2 or 10 m, can be found taking into consideration that the wind velocity logarithmically increases with height from ground level. Figure 8a presents quantities h_C and h_{CR} as functions of the wind velocity v in a range from 1 to 20 m s^{-1}.

Air circulation around a body in the case of free convection either in closed premises or out-of-doors in very calm (windless) weather is determined only by its convective buoyancy obeying the Archimedes principle — that is, by the air density gradient. In many cases, this gradient can be found rather exactly as a function of the temperature gradient at the body surface, created by the difference between skin surface and ambient air temperatures. When T_0 is close to T_a, sweat evaporating from the body surface will contribute to the convective buoyancy of the air. The magnitude of the contribution will be determined by the pressure and temperature differences at the air/skin interface. Under such convection conditions, the heat transfer coefficient is directly related to density variations in the 'vapor–air' system and can be taken into account via *effective temperature*. Let us see how changes in vapor-saturated air density can be taken into consideration by introducing an effective temperature.

The density of saturated water vapor, similar to dry air density, drops with increasing temperature or decreasing pressure because the gas volume grows in accordance with Clapeyron's equation. At room temperatures and normal atmospheric pressure, the density ratio between saturated water vapor and dry air equals approximately 0.62. With the water vapor removed, the air density increases. The *effective temperature* of an air sample is the temperature to which it must be heated to maintain the same density (hence, the pressure p) as that of totally dry air. It can be shown that the effective air temperature T_a^{eff} is related to the real temperature T [K] and vapor pressure e as

$$T_a^{\mathrm{eff}} = T\left(1 + \frac{0.38e}{p}\right). \tag{21}$$

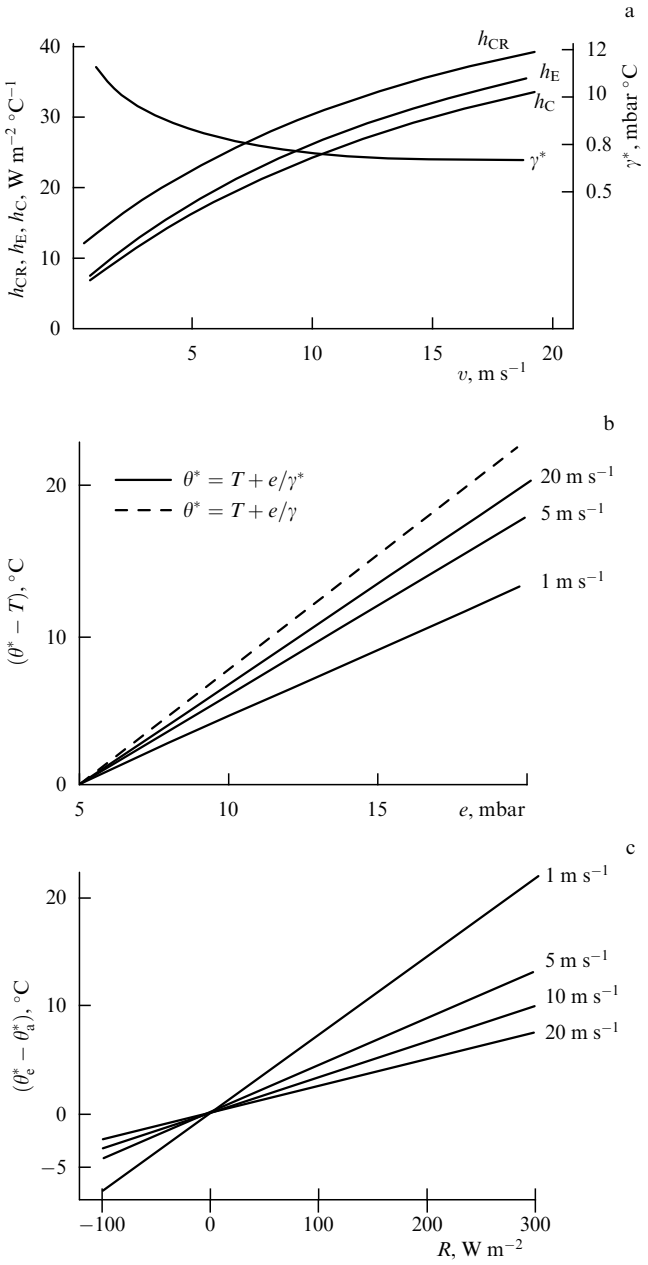

Figure 8. Plots for the calculation of effects of physical environmental factors [velocity of air motion (wind) and humidity] on the temperature of the human body surface: (a) dependences of the parameters h_{CR}, h_E, h_C and γ^* on the wind velocity v, i.e., on the ambient air flowing around body under forced convection conditions; (b) difference between equivalent ambient temperature θ^* and real air temperature T as a function of vapor pressure e at different wind velocities v; (c) dependence of the difference between equivalent (θ_e^*) and real (θ_a^*) air temperatures on the summarized isothermal radiation R at different wind velocities v [19].

For example, dry air with a temperature of 41.7 °C has the same effect on a person as vapor-saturated air having a temperature of 35 °C. In other words, convective buoyancy forces acting on an air sample saturated with water vapor at 35 °C are equivalent to the same forces acting on dry air at 41.7 °C. Those fond of steam-bathing know this fact from their experience: the increased temperature in a dry Finnish sauna is endured easier than in a wet, water vapor-saturated Russian bath-house. The literature contains reports of scientific investigations into this issue, including those with the aid of thermovision technique, but they are not discussed

here. The interested reader is referred to the monograph [49] and references cited therein.

The coefficient h_E is related to the coefficient h_C by the ratio of vapor molecular diffusion coefficients at respective temperatures. When energy is transferred from a high-temperature body through evaporation under forced convection conditions, then $h_E = 1.07h_C$ (Fig. 8a). In this case, the ratio $\gamma^*/\gamma = h_{CR}/h_E$ may be expressed as $0.93 + 4\sigma T^3/h_E$. It decreases to a minimum value of 0.93 as the wind velocity falls off. Figure 8a shows the dependence of γ^* on the wind velocity under forced convection conditions.

The above estimates of mean body temperature variations under the influence of environmental factors are of less importance for the analysis of human IR images in the case of panoramic observations. Diagnosis by this method is based on the qualitative visual scrutiny of an IR image as a whole or the calculation of relative quantitative parameters, e.g., the temperature ratio between a given site at the skin surface and its surroundings (for the diagnosis of venous and arterial pathology) or the ratio of temperatures on the right and left sides of the face in patients with neurologic disorders. These ratios are less sensitive to variations in average skin temperature. At the same time, changes in mean body temperature due to environmental influences need to be determined and taken into account for the purpose of precise radiometric measurements.

4.4 Human temperature indoors and outdoors

It appears appropriate that diagnostic procedures with the use of thermovision devices be carried out indoors, i.e., in the absence of drafts and a direct illumination from thermal devices. However, medical practice not infrequently faces situations where similar measurements have to be made in large glassed buildings at airports and railway stations or out-of-doors.

By way of example, such a necessity arises when quarantine actions are considered during epidemics and when overall analysis on an r.t. basis is needed of IR images of all passengers arriving from regions affected by an infection. The purpose of these procedures is to rapidly identify subjects with certain parameters characteristic of the early stages of a concrete disease. Carriers of abnormal parameters are then subject to a more detailed examination in specialized medical settings, as appropriate, and are put in quarantine, when the occasion requires. Hence, the importance of knowing artifacts likely to be encountered during outdoor thermovision procedures.

A total flux R_{ni} of radiation energy from the warm surroundings, absorbed by the human skin surface, cannot be measured directly. However, it is possible to evaluate it by measuring IR radiation from the skin surface with the help of the procedure described below. Under indoor conditions, this quantity may be regarded as radiation of a blackbody at a certain average wall temperature of the room. The analog of this temperature in outdoor conditions is the mean temperature of radiation from the Earth's surface and atmosphere. The radiation flux can be calculated considering radiation L_u emitted upward from the body surface and atmospheric radiation L_d emitted downward. The mean value of the flux for the walls of a vertical cylinder (model of a human body) is $\bar{L} = (L_d + L_u)/2$. For the walls of a horizontal cylinder simulating a patient placed on a hospital bed, this formula assumes the form $\bar{L} = (1.04L_d + L_u)/2$, where the coefficient 1.04 takes into account the spatial distribution of atmospheric radiation. Such consideration is valid in the absence of local illuminations, i.e., in the case of diffuse irradiation. This situation corresponds to cloudy skies, when measurements are conducted out-of-doors.

For an in-depth analysis of outdoor measurements, account should be taken of three radiation components, viz. direct solar radiation, scattered radiation from the sky and clouds, and diffuse radiation reflected from the foundation surface (a floor or the ground). Each component is possible to assess by multiplying the solar radiation flux S into an appropriate coefficient, with the flux averaged over time and denoted as $\bar{S}$ [44].

In this case, the quantity R_{ni} is defined as

$$R_{ni} = \bar{S}(1 - \rho) + \bar{L} - \sigma T_a^4 , \tag{22}$$

where ρ is the coefficient of reflection from the skin's surface, σT_a^4 is the skin radiation flux density at air temperature T_a, and σ is the Stefan – Boltzmann constant.

In practice, direct and scattered radiation at the horizontal surface can be measured by two spectral radiometers. One of them records both components, while the other is screened from directed solar radiation and measures only diffuse radiation in front of the foundation at a floor or ground level. Up-to-date IR systems do not include radiometers because they make the above measurements automatically.

The equivalent temperature θ^* equaling $T + e/\gamma^*$ depends on the air temperature and humidity, wind velocity, and body geometry. The quantity $\theta^* - T = e/\gamma^*$ is amenable to evaluation because humidity increases in proportion to water vapor pressure and depends on the wind velocity. It follows from Fig. 8b that this dependence is rather weak.

Figure 8c shows the difference between equivalent temperatures of the environment (θ_e^*) and the air (θ_a^*) as a function of total isothermal radiation and wind velocity: $\theta_e^* - \theta_a^* = R_{ni}/h_{CR}$, when the wind velocity is above 5 m s^{-1}.

The real equivalent ambient temperature θ_e^* is calculated by the addition of radiational increment R_{ni}/h_{CR} to θ_a^*. An increase in the difference $\theta_e^* - \theta_a^*$ depends on R_{ni} and the wind velocity. In order to find θ_e^*, when T_a, e_a, R_{ni}, and v are known, the plots in Figs 8b and 8c must be considered together.

The human body is cooled by heat release not only through the skin but also via the respiratory system. It should be recalled that the lungs have a very large surface area, many times that of the body (see Table 5). If T_r is the temperature of the air exhaled from the lungs, and $\dot{V}$ [m^3 s^{-1}] is the normal breathing ventilation rate, then the fall of high temperature is defined as $\rho c_p \dot{V}(T_r - T_a)/P$, where ρ [kg m^{-3}] and c_p [W kg^{-1}] are the air temperature and specific heat capacity, respectively, at the temperature T_a and constant pressure, and P is the body's surface area.

The quantity $h_B = \rho c_p \dot{V}/P$ [W m^{-2} s^{-1}] may be regarded as the coefficient of power loss through the respiratory system from unit area of the body surface per unit time, similar to the coefficient h_C of convective loss of high temperature through the skin. The high temperature loss is defined as $h_B(e_r - e_a)/\gamma$, where e_r is the water vapor pressure in the exhaled air. Now, the total loss of high temperature owing to respiration may be expressed as

$$h_B\left[(T_r - T_a) + \frac{e_r - e_a}{\gamma}\right], \tag{23}$$

where the quantity in the square brackets is the difference of equivalent temperatures between the inhaled and exhaled air

(having temperatures T_a and T_r, respectively) corrected for the difference between their humidities and vapor pressures. In this case, the complete balance equation (6) acquires the form

$$M - W = h_{CR}(\theta_0^* - \theta_a^*) + h_B(\theta_r - \theta_a)\,, \qquad (24)$$

where $\theta_r = T_r + e_r/\gamma$. The analysis may be simplified on the assumption that e_r is the vapor-saturated air pressure at temperature T_r.

Here is an example from Ref. [44] to illustrate the use of these formulas.

Suppose that a subject dressed in light clothes out-of-doors

(1) *is exposed to a wind with an average velocity of* $2\ \mathrm{m\ s^{-1}}$, *and*

(2) *has his or her body heated from inside by a metabolic energy of* $100\ \mathrm{W\ m^{-2}}$.

It is necessary to determine the ambient air temperature T_a *at which the subject does not sweat while the mean temperature at the body surface is maintained at the level, say,* $T_0 = 32\,^\circ C$.

Let us answer this question. It should be recalled that we have a constant body temperature ($\approx 37\,^\circ$C). As much as 15–20% of the metabolic energy in a human is spent to support internal processes (e.g., ATP synthesis). If the net loss of radiation energy in the air is $80\ \mathrm{W\ m^{-2}}$, it follows from Fig. 8a that $h_{CR} = 16\ \mathrm{W\ m^{-2}\,^\circ C^{-1}}$ at a wind velocity of $2\ \mathrm{m\ s^{-1}}$. Hence, the difference of equivalent temperatures between the skin and the air must be $80/16 = 5\,^\circ$C. In the absence of perspiration, the quantity e_0 should be considered equal to e_a, and the radiational increment due to absorption of external radiation by the body surface is $R_{ni}/16$. Therefore, one finds

$$\theta_0^* - \theta_a^* = 32 - \left(T_a - \frac{R_{ni}}{16}\right) = 5\,^\circ\mathrm{C}\,, \qquad (25)$$

so that

$$T_a = 27 - \frac{R_{ni}}{16}\,. \qquad (26)$$

The results following from Eqns (25) and (26) give the answer to the question of interest.

Let us specify the value of R_{ni} more accurate. Under the bright sun, the radiational increment due to radiation absorption by the body surface from the outside may be as high as $R = 200\ \mathrm{W\ m^{-2}}$. Expression (26) gives the air temperature $T_a = 14.5\,^\circ$C. In the shade, one finds $R_{ni} = 20\ \mathrm{W\ m^{-2}}$; therefore, the air temperature (in accordance with the same expression) must be $T_a = 25.75\,^\circ$C.

The result of this computation is not unexpected. Everyone knows from his or her life experience that *comfortable* air temperatures in the sun and in the shade are different for each individual. The above calculations may be helpful for the quantitative assessment of this difference. It is important to remember that the measurement of air temperature alone for the purpose of thermovision diagnosis is insufficient to unambiguously determine whether *given environmental conditions are comfortable for a subject*. Air humidity and radiational increment due to external radiation can also markedly affect results of IR radiometry.

It should be recalled that the human skin viewed from the standpoint of heat carrying capacity constitutes a controllable thermal waveguide, the heat conductivity of which varies in different directions. Also, its thermal conductivity depends on environmental conditions. The average skin temperature of a naked human subject adapted to summer temperatures of Central Russia is usually close to $31.5\,^\circ$C at an indoor air temperature of $22\,^\circ$C or so. Temperatures of exposed parts of the body surface may differ by $7\,^\circ$C. The legs have a minimal temperature ($\approx 27-28\,^\circ$C at the feet), whereas cervical areas close to carotid arteries have a relatively high temperature ($\approx 34\,^\circ$C).

The difference $T_0 - T_a$ grows with decreasing air temperature. The above reference to "the average skin temperature of a naked human subject adapted to summer temperatures of Central Russia" is essential in that comfortable temperatures for the naked residents of northern and southern regions of this country are quite different; the same refers to seasonal comfortable temperatures [29].

Turning back to the above computation of comfortable temperatures for a human being, it needs to be noted that the same formulas may be used to determine them under varying humidity and atmospheric pressure, at different sweating and breathing intensities, in a subject wearing clothes (provided thermal conductivity and radiation absorption of the material are known), etc. These issues are beyond the scope of this review, and the interested reader is referred to the works [44–49] for details.

4.5 Requirements for infrared radiation measurements

The results of the analysis presented in Section 4.4 may be used to formulate requirements for both radiometric procedures and rooms for thermovision diagnostics.

(1) *Temperature should be measured in the thermoneutral zone,* i.e., in the range of *comfortable temperatures* at a constant difference $\theta_0^* - \theta_a^*$ between equivalent temperatures, where θ_0^* is the equivalent temperature of a *selected 'reference' point* at the skin surface, and θ_a^* is the equivalent indoor air temperature. It should be recalled that the equivalent temperature θ^* is equal to the real temperature after introducing correction $T(v)+e/\gamma$ for humidity, air motion, and body geometry. *The 'reference' point for the skin temperature scale of an awake person* (with open eyes) may be the temperature of an orbital cavity close to the bridge of the nose [50] (see Section 7.1); this temperature is relatively stable: $\theta_0^* = 36.5\,^\circ$C. The equivalent comfortable air temperature θ_a^* for a naked subject in a room under normal humidity and pressure in the absence of forced ventilation is on the order of $22-24\,^\circ$C. This value is $1\,^\circ$C lower in winter, so that $\theta_a^* = 22-23\,^\circ$C, and higher in summer, $\theta_a^* = 23-24\,^\circ$C due to a seasonal adaptation of the organism [51].

(2) *Prior to measurement, the patient should be adapted to a temperature similar to that in the examination room.* It takes varying times for the skin of individual patients to acquire the equivalent air temperature of the room. It depends on the age-related intensity of the patient's metabolism, subcutaneous fat thickness, the state of vasculature, and other physiological characteristics (see Table 5), as well as the degree of the patient's cooling immediately prior to the visit, especially in wintertime. The rate of internal heat transfer in the body is not a limiting factor because one complete cycle of blood circulation takes only 1 min. In fact, the limiting factor is sluggishness of the skin heating process. Knowing the balance between the amount of heat transferred through the skin per unit time and that generated in the body, it is possible to estimate characteristic time τ of tissue heating to the temperature θ_0^*:

$$\tau = \frac{c\rho l^2}{\lambda}\,, \qquad (27)$$

where c is the specific mass heat capacity of the skin, ρ is its specific weight, l is the skin thickness, including the subcutaneous fat layer, and λ is the thermal conductivity.

Parameters entering expression (26), including some temperature-dependent ones, vary in the following ranges: $c = (2-4) \times 10^{-3}$ kJ g^{-1} K^{-1}, $\rho = 1.02 \times 10^3$ kg m^{-3}, $\lambda = 0.2-2$ kJ m^{-1} h^{-1} K^{-1}, and $l = (5-10) \times 10^{-3}$ m. The order of values obtained in the evaluation is essential because an exact quantitative estimation of τ does not make much sense in view of marked variations in the aforementioned parameters in individual patients. Substitution of the above values into expression (27) gives a range of τ variations from 3 to 30 min. Bearing in mind the exponential dependence of the heating process, adaptation takes approximately 3τ, i.e., from 9 min to 1.5 h.

Experimental examinations of concrete patients indicate that an outdoor temperature below $-5\,^{\circ}$C requires that an individual be adapted to the indoor temperature for at least 1 h on average if a measurement error during radiometry is to be avoided. Otherwise, the temperatures of certain facial areas are likely to be underestimated, and that of others overestimated. Adaptation is virtually unnecessary in summertime, but the patient must be asked to remove sweat from the body parts to be examined by thermovision devices.

(3) *The patient's posture is of importance*. Infrared images of a subject in the upright and supine positions are unlike for two reasons. First, blood circulates differently in the body of differently positioned people. Second, the human body is a moist object with a higher temperature, which always causes at least weak air convection around it in closed premises. The heat transfer coefficient h_C [see expression (9)] for a subject in the upright position is higher than in a lying person even in the absence of forced convection. Mean dispersion of the measured values, in the limit, may reach 10%.

(4) *The cubic capacity of a room for thermovision diagnosis must be approximately 100 times the total body volume of the two people present* (*the patient and the doctor*). In order to avoid thermal radiation interference between the people and the equipment and exclude transient air convection processes, the room area must be at least 20 m^2; no directed heat flux from lighting or heating equipment is allowed. The walls of the room must be covered with a mat heat-absorbing material.

(5) *It is desirable that a room for thermovision diagnosis be equipped with an air conditioning system*. Such systems substantially extend the application of thermovision for both research and diagnostic purposes, while their cost is much smaller than that of the thermal imaging equipment.

In the comfortable temperature range, we do not sweat and the sweat pores are closed, although moisture continues to be released through the skin surface. However, some patients exhibit abnormal sweating patterns. Increased or reduced perspiration in humans is an indicator of various disorders. Changes in body temperature during intense physical work (*exercise test*) or indoor air heating (*thermal test*) deserve special study [49].

5. Implications of photonic and microbolometric thermal imagers for biomedicine: effects of patients' skin characteristics and spectral range on the results of radiometry

Apart from environmental factors influencing the results of thermographic studies (see Section 4), measurements of temperature also depend on the parameters of IR cameras. First, any IR system for biomedical diagnosis finds wide practical applications only when its cost–effectiveness relation reaches a certain optimal level. The cost of thermal imagers depends on the type of their temperature stabilization units, all other characteristics being equal. Photon cameras cooled by liquid nitrogen are more expensive than microbolometric devices that do not use such cooling. A natural question is what information about the study subject is lost when it is examined using a microbolometric camera. Is it worth equipping diagnostic rooms in hospitals with such instruments?

Second, it has already been mentioned that thermal imagers are most frequently operated in two IR wavelength regions corresponding to atmospheric transparency windows, namely, within 3–5 μm, and 8–12 μm (see Fig. 1). Which of them is more suitable for biomedical diagnosis?

Third, emissive power of human skin varies with the subject's age and physiological condition. The qualitative panoramic examination is virtually independent of skin properties and imager characteristics but they need to be considered in precise radiometry. In an effort of accounting for them, radiometric measurements were made simultaneously with the help of a photon camera cooled by liquid nitrogen and of a microbolometric camera without such a cooling [52]. The aim was to elucidate the effects of spectral range variation and the accuracy of measuring temperature on the efficiency of the diagnosis of different forms of vascular pathology. The study was carried out in a closed room, in the thermoneutral zone, and was focused on the measurement of leg temperature in more than 100 patients suffering limb vascular disorders. Examination was followed by the analysis of IR images of the affected legs (varicosis, atheromatosis) before and after surgical vascular shunting or the replacement of damaged blood vessels with prostheses. IR images were obtained in different wavelength regions using thermovision cameras with a two-fold NETD between them.

One of the two thermal imagers, used by us, had a cooled matrix of indium antimonide-based IR detectors with a spatial resolution of 320×240 elements, an NETD not worse than $0.02\,^{\circ}$C, and a recording rate of 150 frames per second. The camera measured temperature distributions in the IR wavelength region of 3–5 μm.

The microbolometric camera had a vanadium dioxide matrix of the same size as above and a temperature stabilization system using no liquid nitrogen; its NETD was $0.04\,^{\circ}$C at a recording rate of 50 frames per second. The instrument measured temperature in the 8–12-μm wavelength range.

The two cameras were preliminarily calibrated against a blackbody.

It is worthwhile to recall that registering of a human IR image requires that the intrinsic radiation component (isothermal net radiation) and additional radiation induced by the environment should be distinguished at each point on the body.

Power density R_{ni} of isothermal net radiation from a human proper is related to his or her intrinsic temperature T_0. Additional radiation induced by the environment is determined by the air temperature T_a in the room and skin emissive power ε. The latter parameter depends on the properties of the epidermis; its normal value lies in the range $\varepsilon = 0.94-0.98$ and can be as low as $\varepsilon = 0.74$ in the case of skin pathology. In other words, the value of ε is a diagnostic sign of various diseases.

The power density R_{ni} of IR radiation, both induced by the environment and detected by a thermal imager, regardless of its type, is described by the following dependence [53]:

$$R_{ni} = \tau_{atm}\left[\varepsilon f(T_o) + (1-\varepsilon) f(T_a)\right] + (1-\tau_{atm}) f(T_{atm})\,, \tag{28}$$

where R_{ni} is the power density [W m^{-2}], τ_{atm} is the atmospheric transmission coefficient, ε is the emissivity of the object, T_o is the object temperature, T_a is the background temperature, T_{atm} is the atmospheric temperature, and $f(x)$ is the gauge function; here, $\tau_{atm} = \exp(-\alpha d)$, where α is the damping factor [length unit^{-1}], and d is the distance between the object and the camera.

Measurements have shown that the difference in the shape of spectral transmission bands in atmospheric transparency windows for the 3 – 5- and 8 – 12-μm wavelength regions has no appreciable effect on the thermal sensitivity of the imager because the patient is located very close to the camera. This permits us to assume $\tau_{atm} = 1$ when measurements are made indoors. Bearing in mind expression (28) at $\tau_{atm} = 1$ and $f(x) = 1$, regardless of the type of thermal imaging devices, the measured and proper (real) temperatures at each point on the patient's body are related by the following linear dependence:

$$T_{meas} = \varepsilon\theta_0^* + (1-\varepsilon)\,\theta_a^*\,, \tag{29}$$

where θ_0^* is the equivalent temperature of a given body area measured by the thermal imager, and θ_a^* is the equivalent indoor air temperature. It follows from expression (29) that the difference $\theta_0^* - T_{meas}$ may reach several degrees at small values of ε ($\varepsilon \leqslant 0.8$) and relatively low temperatures ($\theta_a^* \leqslant 20\,^\circ$C). For example, at $\theta_a^* = 20\,^\circ$C, $\varepsilon = 0.8$, and $T_{meas} = 35\,^\circ$C, correction amounts to $\theta_0^* - T_{meas} = 38.75 - 35 = 3.75\,^\circ$C. However, this difference does not exceed 0.8 °C at the ε value for normal skin ($\varepsilon \approx 0.95$).

Results of the measurements also depend on the distance between the patient's body and the objective of the IR camera. Correction $\Delta T(d)$, where d is the distance from the objective, depends on its design and the wavelength region within which measurements are made. Anyway, this value is one order of magnitude smaller than corrections for the ε and θ_a^* effects on the process of interest.

Experimental findings indicate that thermal images of humans obtained with calibrated thermovision devices and properly corrected show no dependence on the spectral range — that is, IR images taken at 3 – 5 and 8 – 12 μm are indistinguishable.

Figure 9 depicts thermal images of the legs of two patients, obtained in the visible and IR (3 – 5 and 8 – 12 μm) wavelength regions. By way of example, two extreme cases of varicosis are demonstrated. One is the advanced stage of varicosis requiring urgent medical treatment, with $\varepsilon = 0.82$ (Fig. 9a), and the other is an earlier stage at which varicose veins are inapparent in the visible wavelength range, corresponding to $\varepsilon = 0.95$ (Fig. 9b). Figure 9c presents the respective temperature profiles along the A – A and B – B lines for the 3 – 5- and 8 – 12-μm spectral regions. The appropriate curves practically coincide.

At the same time, it turned out that cameras operated in the 3 – 5-μm range are more responsive to skin reflexes induced by illumination from external thermal radiation sources because their spectral sensitivity better matches skin

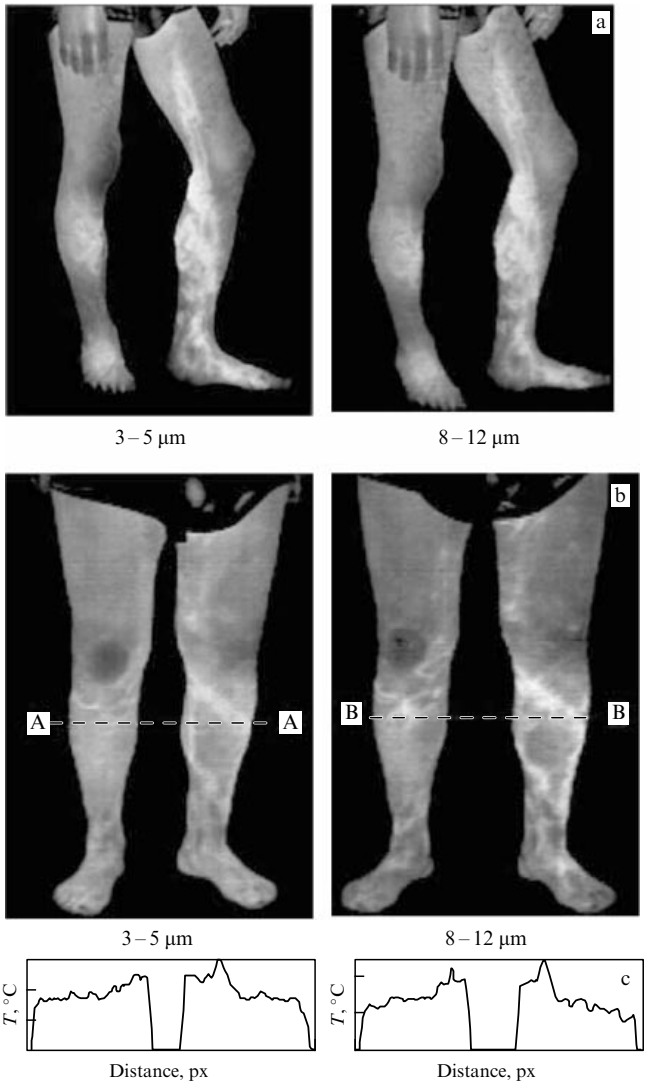

Figure 9. Thermal images of varicosis obtained in 3 – 5- and 8 – 12-μm IR regions: (a) at $\varepsilon = 0.82$, advanced stage, (b) at $\varepsilon = 0.95$, and (c) temperature profiles along the A – A (3 – 5 μm) and B – B (8 – 12 μm) lines.

radiation spectra induced by electrical lighting appliances. The influence of these appliances on 8 – 12-μm cameras is less significant.

It may be concluded that, *with the above requirements duly met, the more cheap microbolometric cameras with vanadium dioxide or amorphous silica matrices operated in the* 8 – 12-μm *wavelength range* (*without cooling by liquid nitrogen*) *may be employed in medicine along with the liq.* N_2*-cooled photonic IR cameras working in a wavelength range of* 3 – 5 μm.

6. Areas of thermovision application in biomedicine

Thermovision happily combines the possibility of visualizing pathological changes and absolute safety for both patients and medical personnel.

To avoid overloading the reader with medical terminology, this paper does not consider numerous clinical cases and is confined to enumeration of thermovision application areas with relevant references to literature sources. It should be emphasized that references to theses [54 – 67], monographs [3,

5, 9, 28, 49, 68–79], reviews [2, 17, 24, 26, 27, 80–84], and journal papers [4, 85–133] published before 1995 are largely concerned with the medical applications of optico-mechanical or film-based thermovision devices rather than matrix systems. However, it does not belittle the importance of these publications since they laid the basis for the further development of thermal diagnosis techniques in biomedicine with the use of matrix thermovision highlighted in the post-1998 literature.

Thermovision finds application in various fields of medical diagnosis, including diabetic angiopathy, atherosclerosis, limb endarteritis, Raynaud's disease, hepatitis, vegetative regulation disturbances, pneumonia, inflammation of accessory nasal sinuses, renal disorders, cystitis, peripheral nerve lesions, arthropathies of different etiology, vertebral pathologies, mastitis, and breast and skin cancer. Also, the use of thermal diagnosis has been described in vascular surgery, neurosurgery, and the evaluation of skin graft viability. Even this long list can be further extended to encompass many other areas of matrix thermovision applications in biomedicine.

There are two views of the diagnostic utility of thermovision.

One ensues from the following postulate. Since a thermal imager records temperature distribution over the skin surface, examination of the human body with the use of IR radiation may be used to evaluate and thoroughly analyze peripheral blood circulation as an important diagnostic criterion. Advocates of this view among doctors maintain that application of thermovision is especially promising for the diagnosis of breast cancer [5, 85–87], vascular disorders and nitrogen oxide synthesis [88–108], blood supply to the brain in patients with craniocerebral injuries, and facial inflammation [109–126] or the viability of grafted tissues [132, 133]. Moreover, they consider thermovision as an important tool for the diagnosis and follow-up of diseases requiring objective blood microcirculation monitoring for their management [127–131]. It is also emphasized that thermovision techniques readily demonstrate the formation of hyperthermic foci in different parts of the body (e.g., breasts or lymph nodes), as well as hypo- and hyperthermal areas in blood vessels, developing at the early stages of certain diseases. These features are frequently missed during routine visual examination in the visible wavelength region or when other methods of early diagnosis are employed. At the same time, there is some doubt that visualization of the skin surface and the resulting IR images invariably provide valuable information about processes inside the body.

Other biomedical researchers adhere to the hypothesis that all normal functions of a healthy subject as well as their abnormalities are in the end reflected in human IR images and can be explained from the results of their detailed analysis. The dynamic range of IR cameras, their space–time resolution, and the precision of temperature measurements still remain the main limiting factors. Variations in IR radiation and the dynamics of temperature patterns in different areas at the human skin surface may be used not only to diagnose peripheral disorders but also to obtain a wealth of information about dysfunction of internal organs. This, however, requires examination of altered IR fields in the 'projections' of these organs onto the skin surface.

'Projection' is a key word here, having a special sense. It is obvious that the surface of an injured visceral organ is characterized by a peculiar thermal pattern and average temperature. Changes in these parameters can be registered only when the organ is exposed during surgical intervention. Thermovision has already been applied to such situations in neuro- and cardiosurgery [77].

It is difficult to establish a cause underlying variations in skin surface temperature, associated with pathology of viscera, because thermal fluxes emitted by splanchnic organs are screened both by circulating blood, which tends to equalize inner body temperature, and by the subcutaneous fat layer and the skin itself. The amount of blood ejected from the heart per 1 m^2 of the body surface for 1 min (cardiac index) ranges $1.9-3.3\ l\ m^{-2}\ min^{-1}$. This accounts for rather small temperature variations registered at the skin surface. Nevertheless, it is possible to measure the *mean thermal* effect of a diseased visceral organ on variations in *average temperature of the body* as a whole. Prior to the advent of thermovision, physicians used to measure mean temperature of a selected body area with a thermometer. Such areas comprised an armpit, a sublingual cavity, an acoustic duct, or the rectum. The normal sublingual and armpit temperatures are $\approx 36.7-36.8\,^{\circ}C$ and $\approx 36.6-36.8\,^{\circ}C$, respectively. Rectal measurements give the highest normal temperature value ($\approx 37\,^{\circ}C$).

When deviation of average temperature from the normal value exceeds the bounds of the permissible physiological range, it may serve as a diagnostic clue to some disease. Additional studies are needed to establish exact diagnosis.

For all that, thermal diagnosis of internal pathologies has good prospects by means of detailed analysis of IR images and temperature-dependent dynamics of receptors of the vegetative nervous system or their groups projected on the skin surface and governing activity of a given visceral organ (e.g., Zakhar'in–Head's zones). In physics, such tasks are regarded as inverse problems in which causes are deduced from effects. Many analyses of this type are actually incorrect because the same sum total of the heat taken up by the skin may be constituted by different sets of components peculiar to heat fluxes emitted by different organs. Speaking figuratively, *this situation is analogous to technical fault detection by analyzing the composition of the waste removed from a plant*.

Human skin exhibits around 200 areas corresponding to the 'projections' of viscera onto the body surface in the form of groups of receptors of the vegetative nervous system (their distribution appears to correlate to acupuncture points).

One would think that thermal noise generated by a mature receptor per one degree of freedom must be negligibly small. In an adiabatically isolated system it equals kT (where k is the Boltzmann constant, and T is the temperature in degrees Kelvin) or reaches only 10^{-16} erg K^{-1}. At 36 °C, the energy is on the order of 10^{-14} erg. In a disease, however, even this small value can be recorded by a thermal imager. If an affected organ activates respective receptors, each of them works at a rate of 10^2 operations per second. In this case, the minimal density of the thermal power emitted by the receptors from an area of 100 μm^2 amounts to $10^{-5}\ W\ m^{-2}$.

Cooled cameras with cadmium–mercury–tellurium-based matrices have threshold sensitivity on the same order. This suggests the possibility, in principle, of recording thermal activity of individual receptor groups despite numerous difficulties created by fluctuations in the thermal background due to the movement of blood in capillary vessels and muscular contraction or related to the spatial resolution and the objective aperture diameter of the IR cameras. Flickering of thermal fields against the averaged temperature back-

ground that changes under the effect of blood movement through the capillary network and muscular contraction can be eliminated by a low-frequency filter, the flicker frequency being an order of magnitude smaller than the receptor operating rate (which ranges from 10 to 100 Hz). It may be hoped that further improvement in thermal imagers and computer algorithms for information processing will facilitate solving these problems. Studies including thermal filter-assisted processing of IR images by means of fast Fourier-transform analysis have been conducted by M Anbar since the 1990s [2, 82].

However, certain symptoms characterizing the vegetative nervous system can be easily detected even today without applying local frequency-amplitude analysis of the heat emitted by individual receptors. It has been observed, for example, that dysfunction of one internal organ or another is reflected in a reaction of the vegetative nervous system, leading to a change in the integrated response of the human organism in various functional tests (exercise, thermal tests, drug tests, etc.). The response to tests may have the form of local skin paleness or reddening, sweating, variable heart rate, or characteristic asymmetry of facial or body IR images. These abnormalities are responsible for IR image dynamics and are readily detected by modern thermovision devices [2].

The quality of the solution to an ill-posed problem depends on the amount of *a priori* information. An inverse problem is usually formulated through the definition of a model of the subject's internal milieu based on the observed characteristic changes of its external IR field; this implies knowledge of an operator for the direct transformation of the above-mentioned model into the corresponding field characteristics at the surface. At one time, such an approach to the analysis of processes in the human body began to be developed by a group headed by Yu V Gulyaev at the Institute of Radioengineering and Electronics, Russian Academy of Sciences [129].

There are many methods for the solution of such problems (statistical methods, pseudoinversion, regularization, the Bachus-Gilbert method, etc.). They are especially well-developed in application to geophysical problems [134] that, meanwhile, have some aspects in common with the ongoing problems encountered by biomedical thermal diagnosis.

To conclude, we have discussed the views of two groups of physicians in respect to the role of thermovision in medicine. These views are complementary rather than conflicting. The second approach remains poorly developed and awaits further extensive biomedical and physical studies, accumulation of new experimental data, and improvement of IR imaging technologies. Such studies are of greatest interest for physicists and biophysicists as opening up prospects for the wider use of thermovision in medicine. Section 7 below illustrates this inference by four examples from our experience.

7. Examples of the application of thermovision devices in biomedical research and diagnosis

7.1 Peculiarities of a temperature distribution around the human eye

The objective of this study was to distinguish an area on the human face having stable maximum temperature in order to use it as a reference in the construction of an individual physiological temperature scale characterizing a given person. Identification of such an area is necessary in the context of practical applications of the method in question for diagnostic and related purposes.

It was found that IR radiation emitted by human eyes glows brighter than that from other parts of the face, even though the eyeballs only have intermittent contact with the environment.

The contact of the eyeball with the outside is frequently interrupted because the eyelid protecting it periodically blinks open and closed. Blinking is a reflex act triggered by any irritation of the conjunctiva. Irritation is followed by reflective eyelid closure with a 40 – 70 ms delay. Nevertheless, temperature in the open eye region rapidly rises to a maximum value (36.5 °C in a healthy subject). This phenomenon can be accounted for as follows. Human eye involves six small but highly active muscles (Fig. 10a) and an extensive blood supply system (Fig. 10b); in addition, there is a lacrimal gland capable of contraction. Both the eye locomotor apparatus and the organ producing watery secretion are covered by the lid, while the eyeball (with an open eyelid) is

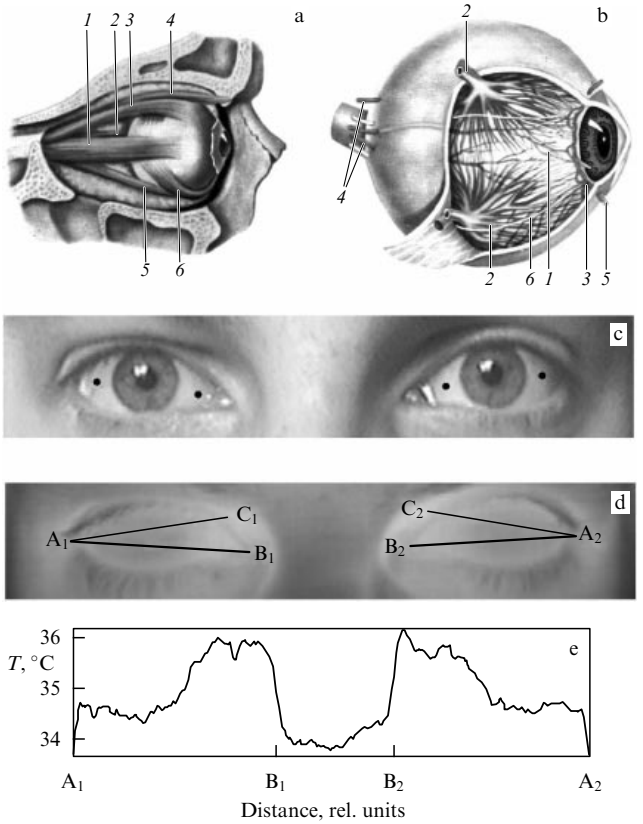

Figure 10. Schematic of the human eye and its image in the visible and infrared spectral regions. (a) Eye muscles: *1* — lateral rectus, *2* — internal rectus, *3* — superior rectus, *4* — superior oblique, *5* — inferior oblique, and *6* — inferior rectus. (b) Blood vessels of the eyeball: *1* — long posterior ciliary artery, *2* — vorticose veins, *3* — greater arterial circle of the iris, *4* — short posterior ciliary arteries, *5* — anterior ciliary arteries, and *6* — ciliary nerves. (c) Eye image in the visible spectral range — black dots denote points where heat production was measured during determination of the eyeball transient thermal characteristic after eyelid opening. (d) Eye image in the IR spectral range with marked lines along which stationary heat production was measured (A_1B_1 and A_2B_2 — lines through the eyeball center for the right and left eyes, respectively; A_1C_1 and A_2C_2 — lines from the temporal edge of the eyelid to its upper part near the bridge of the nose for the right and left eyes, respectively). (e) Thermal profile across both eyes, including the bridge of the nose.

protected by a moist layer and a fibrous membrane. The thickness of the cornea overlying the sclera is relatively small and varies from 0.9 to 1.2 mm between the center and the periphery. In the open eye, the episclera and ciliary body, having profuse vasculature, can emit heat brought in with blood and generated during oxidative metabolism in the eye muscles [135, 136].

We assessed temporal and spatial peculiarities of thermal production in the eyes and the surrounding region in 20 virtually healthy (suffering no apparent pathology) subjects aged 20–65 years.

(1) The transient thermal process was observed in two areas at the eyeball immediately after eyelid opening. One area was near the bridge of the nose, and the other close to the temple (Fig. 10c).

(2) The asymmetry of heat production in the right and left eyes was determined by measuring eyeball temperature along lines A_1B_1 and A_2B_2, respectively, as shown in Fig. 10d.

(3) The hottest eyeball area was identified by measuring temperature along lines A_1C_1 and A_2C_2 from the temporal edge of the eyelid to its upper part near the bridge of the nose for the right and left eyes, respectively (Fig. 10d).

(4) A rise in eyeball temperature relative to those of other facial areas was evaluated.

Measurements as per p. 1 demonstrated that the shape of the curves characterizing the transient processes of a vitreous body cooling with time (after eyelid opening) is highly specific in each person; in the first approximation, it can be described by the expression

$$T(t) = (T_1 - T_2)\left(1 - \frac{t}{\tau}\right)\left(1 + A\cos\frac{2\pi t}{\tau}\right) + T_2\,, \quad (30)$$

where $T(t)$ is the eyeball temperature, T_1 is the eyeball temperature immediately after eyelid opening, T_2 is the stationary temperature of the open eyeball, τ is a characteristic constant determined by the time interval during which the eyeball temperature T_1 after the lid opening drops to a new stationary value T_2, t is the time in the range of $\tau \geqslant t \geqslant 0$, and A is a dimensionless coefficient characterizing the adaptive dynamics of blood vessels and the state of the eye moistening system and ranging $0 \leqslant A \leqslant 0.25$. At $A = 0$, expression (30) takes the form

$$T(t) = (T_1 - T_2)\left(1 - \frac{t}{\tau}\right) + T_2\,. \quad (31)$$

Figure 11 shows a typical measured reaction of the right and left eyes in one patient that conforms to expression (30). At room temperature (22–23 °C), the vitreous body cools by approximately 1 °C from the initial temperature within 5 s after lid opening. Its surface temperature increases within the next 5 s to values 0.3–1 °C higher than the final temperature. Thereafter, the temperature gradually decreases to the final stationary level reached during 10 s; thus, the total duration of the transient eyeball-temperature process is $\tau \approx 20$ s.

The study revealed maximum eyelid temperature close to the bridge of the nose (lid points C_1 and C_2 in Fig. 10d); these points can be used as references in the construction of an individualized physiological temperature scale for the face of a given subject. This temperature fairly well correlates to the corresponding (right/left) temperature in the acoustic duct measured by an infrared radiation thermometer. Temperature in the inner corner of the eye adjoining the bridge of the nose differs from that in the acoustic duct by 0.5 °C at most (spread from 0 to 0.5 °C). The temperature around the pupil is lower than the maximum temperature (when the eye is open for 5–10 s and the person does not blink). Moreover, observations show that the pupil may be regarded as a region of the most uniform temperature distribution (standard deviation from 0.06 °C to 0.15 °C); as such it may serve a reference zone with relatively uniform temperature distribution over the surface.

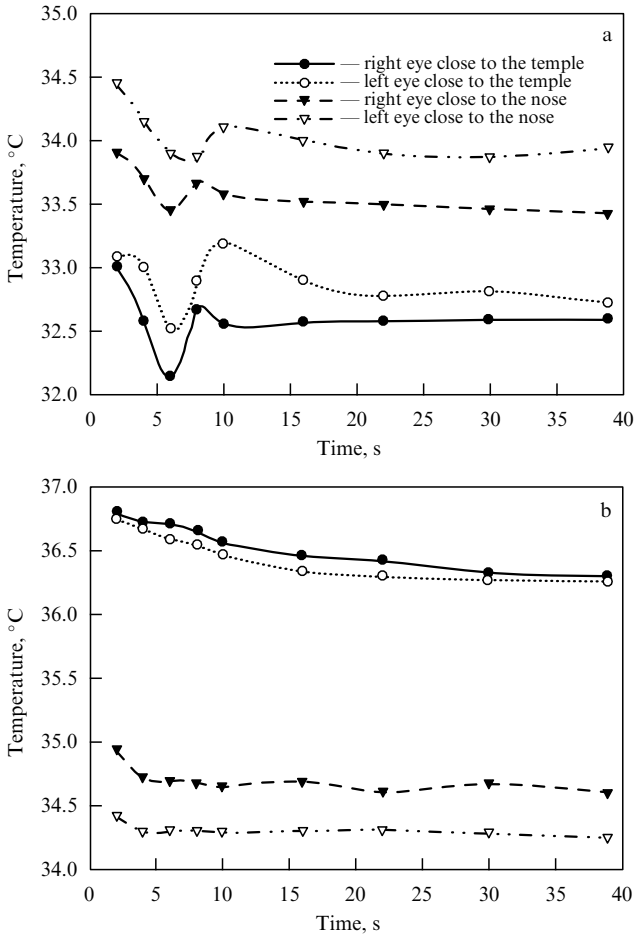

Figure 11. Examples of transient cooling processes at the surface of the right and left eyes after their opening in two people: (a) oscillatory process, and (b) linear process.

Figure 12a illustrates transformation of a facial thermal image at different levels of temperature discrimination counted from the maximum registered value. Figure 12b presents IR images of 12 people cross-sectioned at a discrimination threshold of 0.9 relative to the maximum temperature T_{max}. All healthy people can be arbitrarily categorized into two groups. One includes subjects in whom IR radiation causes only the eyes to glow at the $0.9T_{max}$ discrimination level (six bottom images in Fig. 12b). In the second group, the labial region, as well as the eyes, glows (six top images in Fig. 12b). This means that the choice of the discrimination level does not necessarily guarantee distinguishing the eyes alone. The result depends not only on individual peculiarities of the eyes but also on specific labial blood supply features. The lips are always the hottest part of the face when the eyes are closed.

It appears appropriate to recall a well-known fact in connection with these findings. Tropical habitats of South

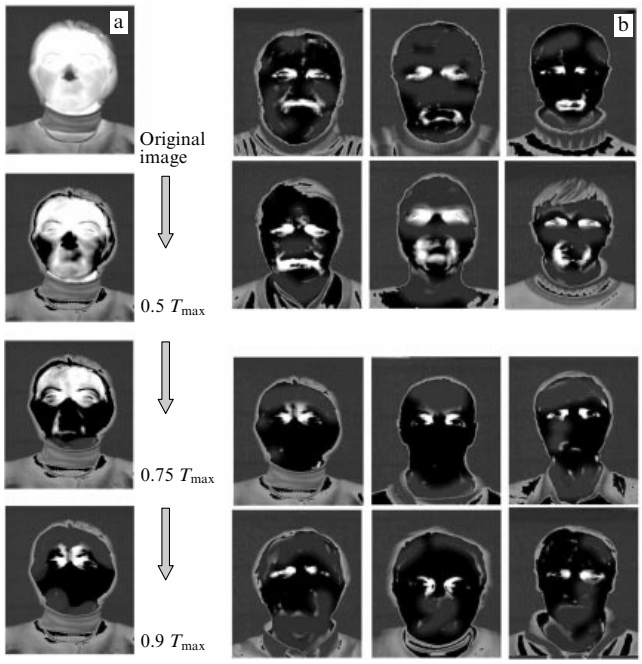

Figure 12. Human thermal images transformed by cross-sectioning their thermal reliefs at different temperature thresholds: (a) example of thermal image transformation at different threshold temperatures relative to individual maximum facial temperature T_{max}; (b) two groups of images of different people obtained at a discrimination threshold of $0.9T_{max}$.

and Central America are home to the assassin bug (*Rhodnius prolixus, Triatomidae*). Its sting is not totally harmless because the bug is a Chagas's disease vector. The insect is sensitive to IR radiation. Scanning the host's skin with its proboscis, the bug makes its way to the warmest area on the open face of a sleeping person, where blood vessels come especially close to the surface. Since the lips have the highest temperature, the insect plunges the proboscis into one of them. Hence, its other name, kissing bug.

Does a diseased eye produce an IR image different from a normal one? Eye conditions provide an important diagnostic clue to the general state of human health [135, 136]. Eyes respond to both infectious diseases and functional disorders of many viscera. Oedema and reddening of the eyes, as well as abnormal intraocular pressure, reflect dysfunction of the nervous and endocrine systems, disturbances of blood supply and haemopoiesis, digestive disorders, renal pathology, and the presence of infection. However, symptoms of diseases become apparent in the visible wavelength region only after serious pathological changes develop in the body. Their early diagnosis is easier to establish by detecting minor deviations from normal temperature in the IR region. True, further studies are needed to address this issue.

Thus far, the available research data allow the following conclusion to be drawn: *the eye region adjacent to the bridge of the nose has the highest temperature and can serve as a reference for the construction of an individualized temperature scale characterizing the face of a given person.*

7.2 The effect of holding one's breath on human thermal image

There is a widespread belief that we can change body temperature by controlling respiration. We decided to verify this assertion by examining 30 apparently healthy subjects of either gender aged 20 – 69 years and differing in response to the breath test. Each was asked to take at least 5 consecutive deep inhalations and exhalations and hold his or her breath after the last inhalation for 25 – 30 s [137].

Figure 13 exemplifies a thermal image of a young woman viewed at different angles (Fig. 13a) and changes in temperature in different facial areas (indicated by numerals) at natural (Fig. 13b) and metronome-driven (Fig. 13c) respiratory rhythms maintained for 3 min. Normal resting respirations in an adult are 16 – 18 breaths per minute. The respiration rate is approximately 4 times lower than the pulse rate. The period of a regular breathing rhythm was chosen to be close to the average one in a given subject. It should be noted that temperature variations in the carotid artery region (area *1*) were modulated by the respiration rate well apparent in the figure.

Figure 14 presents typical thermal images of four patients showing characteristic individual features along with temperature curves for the forehead and carotid artery areas, obtained in a 1.5-min long breath test. Vertical lines show the breath holding zone. It can be inferred (Fig. 14a – d) that initial temperatures in the carotid artery region (curve *2*) are different in individual patients (33.0, 36.1, 33.5, and 35.75 °C). The same is true of forehead temperature (33.6, 35.8, 33.0, and 36.55 °C, curve *1*). Comparison of different

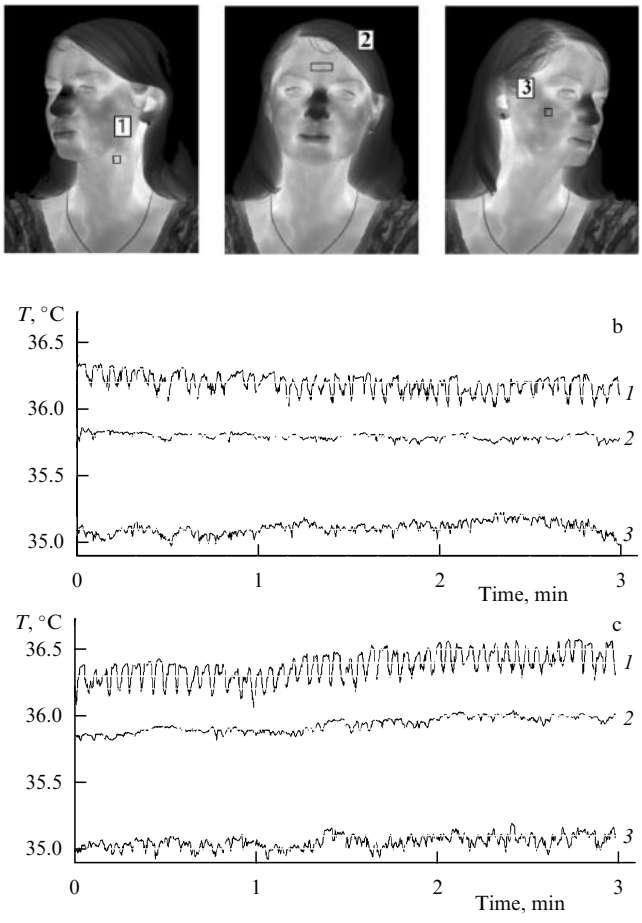

Figure 13. Typical thermal image taken under normal conditions from different perspectives in the 3 – 5-μm IR wavelength region (a). Time-related temperature variations at three facial points at natural (b) and metronome-driven (c) breathing rhythms.

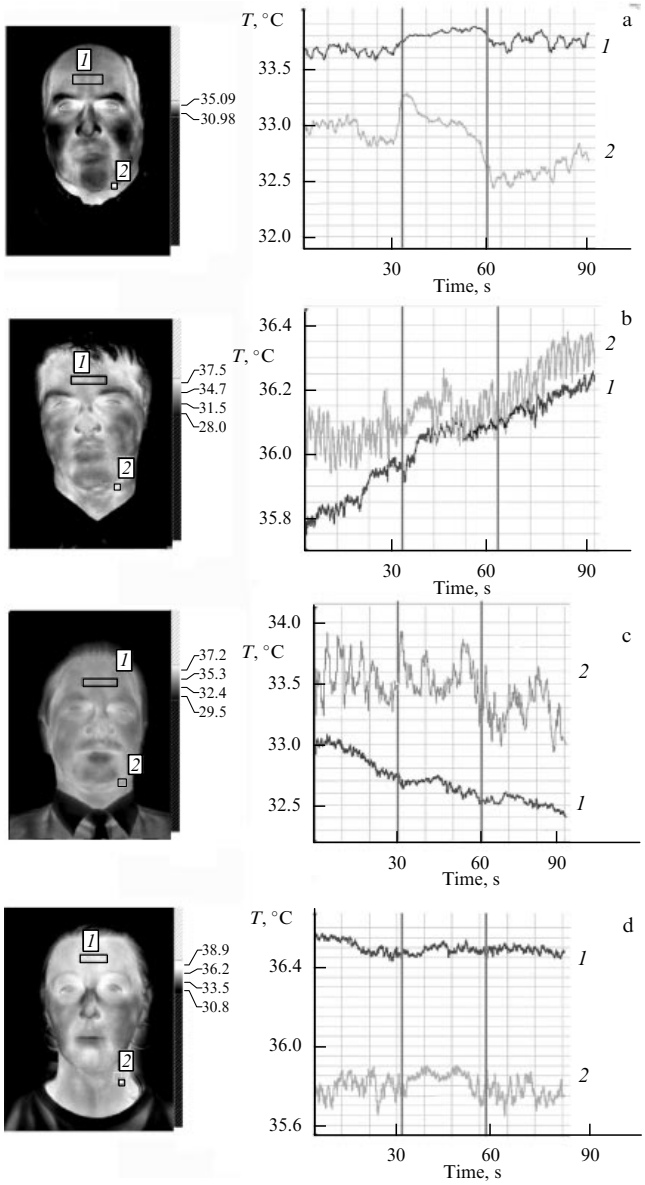

Figure 14. Thermal images of four subjects and the corresponding plots of time-related changes in the breath test: forehead temperatures (curves *1*), and temperatures in the carotid artery region (curves *2*). Vertical lines show the time interval of breath holding: the first one corresponds to the onset of breath holding on inhalation, the second to its termination on exhalation.

thermal images revealed maximum spread of initial temperatures in the carotid artery and forehead regions on the order of $\pm 1.55\,^{\circ}C$ and $\pm 1.53\,^{\circ}C$, respectively. Signs of the derivative of time-related temperature variations were also different in individual patients. Some of them experienced practically no temperature variations (Fig. 14a, d), while in others the temperature either increased (Fig. 14b) or decreased (Fig. 14c).

The difference in the signs of the temperature derivative in individual patients can be accounted for by the fact that each person has a specific pool of rhythms of natural temperature changes ('biological clocks' [51]) with a total amplitude of $\pm 0.7\,^{\circ}C$ with respect to the average value of slowly drifting temperature. For this reason, the sign of the derivative of the curve observed within a short time interval (90 s) depends on the stage of slow natural temperature variations (either rise or fall) at which measurements were made.

It appears from the plots (see Fig. 14) that temperature variations caused by holding one's breath (see the interval between vertical lines in the figure) are much smaller than those conditioned by their natural diurnal rhythm. In the study under discussion, the forehead/carotid artery temperature ratio varied in a range of 0.98 to 1.03. This ratio may be regarded as a physiological norm.

Thus, respiratory rhythm variations within a normal range cause no appreciable change in facial temperature. This can be accounted for by the interaction of two mutually compensatory mechanisms in the respiration process. One of them leads to a rise in temperature, and the other to its fall. The predominance of either mechanism is responsible for the slight corresponding change in the facial IR image of a given person.

The individual characteristics of human subjects are of great importance in this context. For example, temperature variations associated with holding one's breath in the breath test were negligible in mountain-dwelling subjects compared with other participants in our study. The majority of mountain dwellers are known to have enlarged lung capacity, greater inhalation volume, and slightly hypertrophic right ventricle of the heart. A similar type of temperature dynamics is observed in highly trained athletes having a well-developed respiratory system.

Results of temperature measurements of the exhaled air are indicative of lung cooling by expiration. As the hot and moist air being expired enters the trachea, it begins to cool down and part of the water it contains undergoes condensation in air passages. This process as a whole proceeds with an expenditure of heat.

Lung ventilation during normal respiration is effected by active inhalation and passive exhalation. In deep breathing during a breath test, unlike normal breathing, both phases (inspiration and expiration) are active because both involve muscular contraction. Due to this, the air is vigorously blown through the lungs during each breath and leads to body cooling. At the same time, the active work of the diaphragm

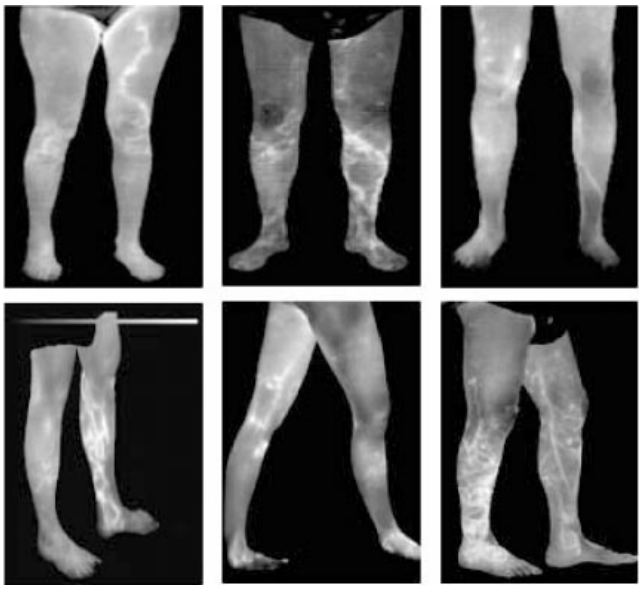

Figure 15. Examples of IR images obtained during panoramic examination of several patients with vascular pathology of the lower limbs.

muscles is accompanied by a slight increase in heat production.

It is worthwhile to note that holding one's breath on inhalation is likely to be of physiological significance. Under normal conditions, however, only 20% of human lung volume is involved in respiration. About 1,500 ml of the air enters the lungs with a deep breath. This amount is sufficient for a trained subject to subsequently hold their breath for 2.5 min (professional divers remain underwater as long as that). This regulatory mechanism is supplemented by cardiac rhythm regulation. In certain subjects, prolonged breath holding is associated with something like bradycardia (slowing of the heart rate). However, the above phenomena do not develop in the case of accidental breath holding.

The forehead/carotid artery temperature ratio computed from experimental observations for healthy people is practically constant, amounting to 1.005 ± 0.025. Experimental findings indicate that *moderate breath holding* (*for* 30 s) *in breath tests does not cause appreciable changes in human thermal images*.

7.3 Thermovision diagnosis of vascular pathology

Arteritis and varicosis are highly widespread vascular disturbances. The number of people with these pathologies is great but differs almost two-fold in different countries. It is estimated at 25% of the total population in Japan, 35% in USA, 53% in Europe, and 50% in Russia. Early diagnosis of these disturbances spares 70% of the patients the trouble of surgical intervention and allows them to confine treatment to drug therapy.

Thermovision provides a highly efficacious tool for the diagnosis of these disorders. Over 1,000 patients were examined using this technique in the Surgical Department, I M Sechenov Moscow Medical Academy. The results are reported in a thesis for the degree of Candidate of Medical Sciences [67]. Figure 15 presents thermal images of several patients with varicose veins. One more example shown in Fig. 16 demonstrates the efficiency of thermovision as a follow-up method for patients with surgically treated atheromatosis. It can be seen that successful substitution of an arterial segment in the right leg resulted in the restoration of

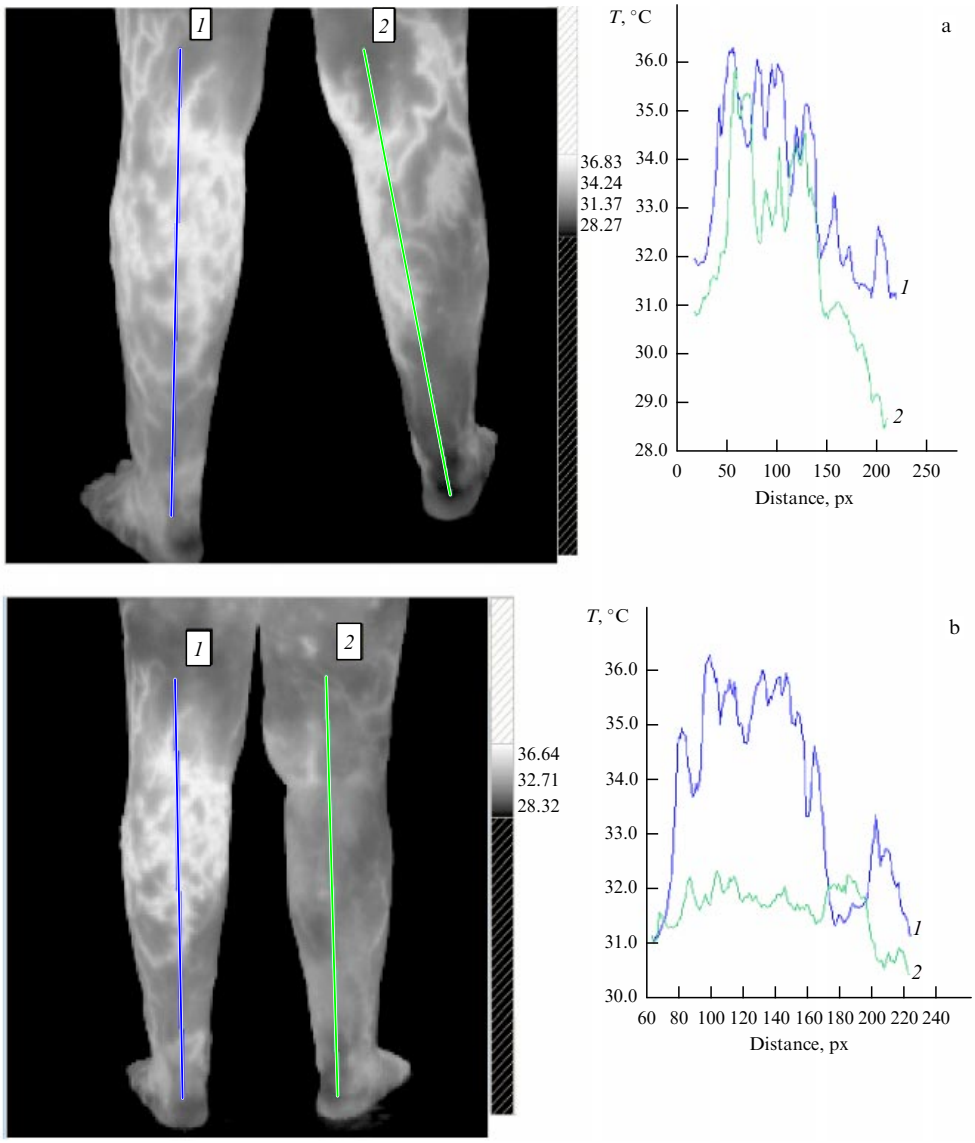

Figure 16. Thermal images of human legs with arterial abnormalities and thermal profiles along lines *1* and *2*: (a) prior to surgical substitution of the arterial defect in the right leg; (b) after surgery. Curves *1* and *2* — thermal profiles from the left and right legs, respectively. The IR image obtained after arterial reconstruction in the right leg demonstrates restored blood flow and cessation of pathological heat release.

normal blood flow, evidenced by the cessation of pathological vein glowing.

7.4 Monitoring the curative process

Patients who received drug therapy for the management of atheromatous lesions in the capillary walls of their lower extremities were followed up with the use of thermovision techniques at the Rehabilitation Centre, Department of Management of the President, Russian Federation [138, 139].

A sharp fall in their leg temperature reflects impaired blood supply associated with microcirculatory dysfunction and pain (sometimes very strong) when walking. Obstruction of microcirculation may be due to a variety of pathological factors including atheromatous intrusion into the capillary lumen.

More than 20 years ago, we developed *perftoran*, a gas-transporting blood substitute in the form of perfluororganic emulsion. Its commercial production was started in 1997 by Perftoran Co., Pushchino, Russia. Each particle of the emulsion contains perfluorodecalin, $C_{10}F_{18}$ (2/3 of the total perfluorocarbohydrate composition weight), perfluoromethyl cyclohexylpiperidine ($C_{12}F_{23}N$, 1/3 of the total weight), and proxanol-268 (a mixture of oxyethylene and oxypropylene) as a surfactant. The particles measure 0.03–0.15 μm [41, 140–146]. Perftoran maintains oxygen transport from lungs to other organs and tissues by virtue of its own oxygen-carrying capacity and rheological properties (small size and large total surface of the particles). Perftoran is used to improve blood microcirculation, apart from many other medical applications (management of hypoxia and ischemic states of different etiology, organ conservation for transplantation, myocardial protection during dry open-heart surgery, etc.) [140, 142, 144].

The particles of perftoran emulsion are made more than 100 times smaller than erythrocytes to facilitate their penetration even into strongly spasmodic capillaries and, thus, the delivery of oxygen to the target tissues. Also, perftoran promotes NO synthesis and the opening of spasmodic capillaries, whereby it ensures progressive substitution of CO_2 for O_2 [146]. Moreover, particles of perftoran serve as a sorbent that cleans up capillary walls and thus widens the vascular channel. Even a minor improvement of oxygen transport, resulting from the restoration of normal blood plasma flow through capillary vessels, may be sufficient for the reversal of the ischemic process.

The study included over 20 patients and a control group of subjects who did not receive perftoran. Administration of perftoran invariably improved blood circulation in lower extremities. The beneficial effect lasted several months or was stable enough for a longer period to make repeated administration unnecessary. Figure 17 compares IR images of the legs of a patient with disturbed blood microcirculation before (Fig. 17a) and two days after (Fig.17b) perftoran administration. Figure 18 illustrates temperature dynamics in different parts of the leg prior to and after perftoran administration. Evidently, the treatment improved blood circulation in capillary vessels and increased foot temperature by more than 2 °C. The follow-up examination of the same patient 6 months later revealed a persistent improvement and the absence of pain. These results published three years ago are now well known in medical circles. Today, perftoran is used to improve blood microcirculation in many clinics in this and other countries [40].

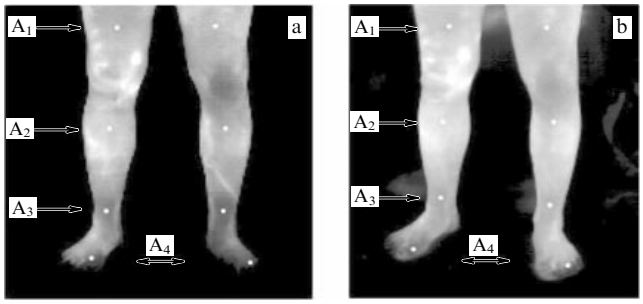

Figure 17. Thermal image of lower extremities with disturbed blood microcirculation: before (a) and two days after (b) perftoran administration. Checkpoints (for four different levels, $A_1 - A_4$) at which temperature was measured.

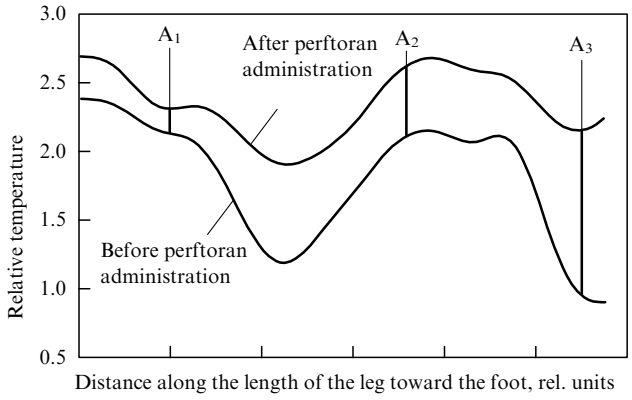

Figure 18. Distribution of relative temperature along the central line of one (right) leg before and after perftoran administration. Temperature values at each point are averaged in the 10×10 pixels region. The zero point corresponds to 31 ± 1 °C.

8. Conclusions

The objective of this review was to demonstrate, in the physical and partly biomedical context, that the development of matrix thermovision created a new scientific discipline, *applied biomedical thermology*, at the borderline of thermodynamics, biophysics, bioinformatics, and radiobiology. The aforesaid material may be regarded as an introduction to this field of research.

The advent of matrix thermovision has brought into biomedicine a rapid, noninvasive, painless, and safe method for the in-depth study of human body functions. Moreover, it opened up new possibilities for obtaining reliable information about human pathology and exposed health problems to be managed with the help of other ancillary diagnostic tools.

Thermovision has good prospects to become an information technology with wide use in biomedicine. Elucidation of all its potential biomedical applications is a subject matter of research anticipated in the very near future.

Worthy of note is another interesting aspect of the aforementioned studies, which pertains to another field of science — psychophysiology. In the beginning, we encountered difficulties in identifying even familiar people from their IR images. The ability to recognize them came with experience. Finally, we learnt how to guess an IR image of a concrete person from his or her color picture obtained in the visible wavelength region and vice versa.

It needs to be emphasized that the developments in matrix thermovision not only signify an important breakthrough in medicine and technology but also give cause to ponder the ways opening for mankind as it enters the technocratic and science-intensive 21st century. The world visible to the human eye is completely unlike the world of the bee or the ant, the frog or the dragonfly. Some animals are color-blind, others have difficulty in seeing motionless objects, for still others the world is as flat as a TV screen. However, the loss of one world dimension is compensated for by the acquisition of another. Is humanity destined at one time or another to take in at a glance the entire world in all its diversity of spectral and dimensional manifestations relying on intellect and developing matrix technologies to extend its perceptive abilities? Is this not totally utopian?

It is probably possible to create a perfect synthesizer of various world pictures and integrate them by some intricate device into one image on a dimensional monitor screen. However, is it within the capabilities of a human being to perceive such an integrated world picture? Is the analytical apparatus of our brain adequate for the task? Perhaps some insurmountable constraints will be imposed, and it will be simply beyond our power to realize what we see.

Moreover, even the world picture produced by our sensory organs is differently perceived and interpreted by individual subjects. Each one of us lives in his or her personal world. Two people (unless they are clones like monozygotic twins) will never have a single meaning of a synthesized world picture. Finally, we must be sure that technical innovations do not lead us up a blind alley but actually extend the human physical senses.

Thus far, advances in thermovision have opened up good prospects for the interpretation of human IR images and extended our sensory perception. We have already learned to derive practical benefits from this technology. This inspires optimism even if it gives no answers to the above questions.

This work was done in the framework of the Program 'Fundamental Sciences to Medicine', Russian Academy of Sciences (Project "The development and improvement of diagnostic methods and tools"). It was partly supported by a grant from the Ministry of Industry and Science, Moscow region, and by the Government of Moscow.

Acknowledgments. The author acknowledges the participation of A A Deev, I B Krest'eva, E P Khizhnyak, and L N Khizhnyak (Cabinet of System Biothermography, Institute of Theoretical and Experimental Biophysics, RAS).

The author also thanks all organizations that rendered support to this work and researchers actively involved in the studies. Thanks are also due to the reviewer of this paper for a number of valuable comments.

References

1. Adams F "Hippocratic writings", in *Great Books of the Western World* (Editor-in-Chief R M Hutchins) Vol. 10 *Hippocrates. Galen* (Chicago: W. Benton, Encyclopedia Britannica Inc., 1952) p. 66
2. Anbar M, Gratt B M, Hong D *Dentomaxillofac. Radiol.* **27** 61 (1998)
3. Vincent J D "Radiometry", in *Fundamentals of Infrared Detector Operation and Testing* (New York: Wiley, 1990) Ch. 3
4. Lawson R *Can. Serv. Med. J.* **13** 517 (1957)
5. Lloyd J M *Thermal Imaging Systems* (New York: Plenum Press, 1975) [Translated into Russian (Moscow: Mir, 1978)]
6. Ivanitsky G R, Litinskaya L L, Shikhmatova V L *Avtomaticheskii Analiz Mikroob'ektov* (Automatic Analysis of Microobjects) (Moscow: Energiya, 1967) p. 75
7. Miroshnikov M M *Teoreticheskie Osnovy Optiko-Elektronnykh Priborov* (Fundamentals of Optoelectronic Devices) 2nd ed. (Leningrad: Mashinostroenie, 1983)
8. Bedford R E "Thermometry", in *The New Encyclopedia Britannica* Vol. 11, 15th ed. (Chicago, Ill.: Encyclopedia Britannica, Inc., 1992) p. 702
9. Gaussorgues G *La Thermographie Infrarouge. Principles, Technologies, Applications* (Paris: Lavoisier, 1984) [Translated into Russian (Moscow: Mir, 1988)]
10. Crowe D G et al. "Theoretical description of photon detectors", in *The Infrared and Electro-Optical Systems Handbook* (Executive Eds J S Accetta, D L Shumaker) Vol. III (Ed. W D Rogatto) (Bellingham, Wash.: SPIE Press, 1993) p. 66
11. Gaussorgues G *Infrared Thermography* (Microwave Technol. Ser., Vol. 5) (London: Chapman & Hall, 1994) Sec. 3.7.2
12. Makarov A S, Omelaev A I, Filippov V L *Vvedenie v Tekhniku Razrabotki i Otsenki Skaniruyushchikh Teplovizionnykh Sistem* (Introduction to the Methods of Development and Assessment of Scanning Thermal Imaging Systems) (Kazan': Unipress, 1998)
13. Kovalev A V, Fedchishin V G, Shcherbakov M I *Spetsial'naya Tekh.* (3) 13; (4) 19 (1999)
14. Koshchavtsev N F, Fedotova S F *Priklad. Fiz.* (2) 141 (1999)
15. Erofeichev V G *Opt. Zh.* (2) 12 (1995) [*J. Opt. Technol.* **62** 73 (1995)]
16. Agranov G A et al. *Opt. Zh.* (9) 53 (1996) [*J. Opt. Technol.* **63** 684 (1996)]
17. Anbar M "Fundamentals of computerized thermal imaging", in *Quantitative Dynamic Telethermometry in Medical Diagnosis and Management* (Boca Raton: CRC Press, 1994) Ch. 4, p. 99
18. Pevtsov E, Chernokozhin V *Elektron. Komponenty* 1 (32); (2) 30; (3) 12 (2001)
19. Sondaevskii V P et al. *Mikroelektronika* **26** (3) 202 (1997) [*Russ. Microelectron.* **26** 172 (1997)]
20. Breen T B et al. *Proc. SPIE* **3436** 530 (1998)
21. Pengelley R, Hewish M *Jane's Int. Defense Rev.* **34** (10) 49 (2001)
22. Andresen B F, Shepherd F D (Eds) *Infrared Technology XIX* (Proc. SPIE, Vol. 2020) (Bellingham, Wash.: SPIE Press, 1993)
23. Ushakova M B *Teplovizory na Osnove Neokhlazhdaemykh Mikrobolometricheskikh Matrits: Sovremennoe Sostoyanie Zarubezhnogo Rynka i Perspektivy Razvitiya* (Thermal Imagers with Uncooled Microbolometric Matrices: Current State of Foreign Market and Prospects of Development) (Moscow: ONTI GUP NPO 'Orion', 2001)
24. Anbar M "Dynamic area telethermometry of skin", in *Quantitative Dynamic Telethermometry in Medical Diagnosis and Management* (Boca Raton: CRC Press, 1994) p. 133
25. Anbar M *Med. Electron.* **147** 73 (1994)
26. Anbar M *Proc. SPIE* **2473** 312 (1995)
27. Anbar M *Med. Electron.* **146** 62 (1994)
28. Vorob'ev L P, Shestakov V A, Egil'skaya V I *Teplovidenie v Meditsine* (Thermovision in Medicine) (Moscow: Znanie, 1985)
29. Petrovskii B V (Editor-in-Chief) *Populyarnaya Meditsinskaya Entsiklopediya* (Popular Medical Encyclopedia) (Moscow: Sovetskaya Entsiklopediya, 1980) p. 471
30. Lightfoot E N *Transport Phenomena and Living Systems*; *Biomedical Aspects of Momentum and Mass Transport* (New York: Wiley, 1973) [Translated into Russian (Moscow: Mir, 1977)]
31. Meshalkin E N et al. *Nestatsionarnyi Krovotok u Cheloveka v Iskusstvennykh Usloviyakh* (Nonstationary Blood Flow in Man under Artificial Conditions) (Executive Editor V S Sergievskii) (Novosibirsk: Nauka, 1984) p. 195
32. Potapova T V *V Mire Nauki* (3) 40 (2006)
33. Lehninger A "Energy conversion in the cell", in *Zhivaya Kletka* (Living Cell) (Ed. G M Frank) (Moscow: Mir, 1966) p. 31
34. Zaalishvili M M *Fiziko-khimicheskie Osnovy Myshechnogo Sokrashcheniya* (Physical and Chemical Principles of Muscular Contraction) (Tbilisi: Metsniereba, 1971)
35. Kramarova L I et al. "The search for and investigation of peptide regulators of hibernation in mammals", in *Recent Research Developments in Endocrinology* Vol. 4, Pt. 2 (Trivandrum, India: Transworld Research Network, 2004) p. 227
36. Rubner M *Die Gesetze der Energieverbrouches bei der Ernährung* (Leipzig: Fr. Deuticke, 1902)

37. Lamb M J *Biology of Ageing* (Glasgow: Blackie, 1977) [Translated into Russian (Moscow: Mir, 1980)]
38. Prosser C L (Ed.) *Comparative Animal Physiology* 3rd ed. (Philadelphia: W.B. Saunders, 1973) [Translated into Russian: Vol. 2 (Moscow: Mir, 1977) p. 140]
39. Winslow R M *Br. J. Haematol.* **111** 387 (2000)
40. Winslow R M (Ed.) *Blood Substitutes* (Boston, Mass.: Elsevier, 2005)
41. Maevsky E I et al. "Perftoran", in *Blood Substitutes* (Ed. R M Winslow) (Boston, Mass.: Elsevier, 2005) p. 288
42. Lindbom L, Tuma R F, Arfors K-E *Microvascular Res.* **19** 197 (1980)
43. Shatsova E N, Dobrodeeva L K, Popov V A *Sovremennye Metody Diagnostiki Zabolevanii Shchitovidnoi Zhelezy* (Modern Methods of Thyroid Gland Diagnosis) (Leningrad: LSGMI, 1985)
44. Monteith J L "Specification of the environment for thermal physiology", in *Heat Loss from Animals and Man* (Eds J L Monteith, L E Mount) (London: Butterworths, 1974) Ch. 1, p. 1
45. Kerslake D *The Stress of Hot Environments* (Monographs of the Physiological Soc., No. 29) (Cambridge: Univ. Press, 1972)
46. Gagge A P "Effective radiant flux", in *Physiological and Behavioral Temperature Regulation* (Eds J D Hardy, P A Gagge, J A J Stolwijk) (Springfield, Ill.: Thomas, 1970)
47. Monteith J L *Principles of Environmental Physics* (London: Edward Arnold, 1973)
48. Sibbons J L *J. Appl. Physiol.* **21** 1207 (1966)
49. Vainer B G *Matrichnoe Teplovidenie v Fiziologii*: *Issledovanie Sosudistykh Reaktsii, Perspiratsii i Termoregulyatsii u Cheloveka* (Matrix Thermovision in Physiology: Investigations of Vascular Reactions, Perspiration and Thermoregulation in Man) (Novosibirsk: Izd. SO RAN, 2004)
50. Ivanitskii G R *Dokl. Ross. Akad. Nauk* **398** 709 (2004) [*Dokl. Biol. Sci.* **398** 367 (2004)]
51. Aschoff J (Ed.) *Biological Rhythms* (Handbook of Behavioral Neurobiology, Vol. 4) (New York: Plenum Press, 1981) [Translated into Russian: Vol. 1 (Moscow: Mir, 1984)]
52. Ivanitsky G R et al. *Dokl. Ross. Akad. Nauk* **407** 258 (2006) [*Dokl. Biochem. Biophys.* **407** 59 (2006)]
53. Altair Manual S9901.D01. Rev A (Croissy-Beaubourg, France: CEDIP Infrared Systems, 2004) p. 51
54. Posherstnik L S "Temperaturnye reaktsii mozga i kozhi u neirokhirurgicheskikh bol'nykh v operatsionnom periode", Thesis for Candidate of Med. Sci. (Simferopol': Crimea State Medical Institute, 1966)
55. Chebotarenko A T "Narushenie termoregulyatsii v ostrom periode cherepnomozgovoi travmy" ("Disturbed thermoregulation in acute cranio-cerebral injury"), Thesis for Candidate of Med. Sci. (Kishinev: Kishinev State Medical Institute, 1968)
56. Strel'tsova E N "Metody termografii i ul'trazvukovoi dopplerografii v kontrole za lecheniem bol'nykh s porazheniyami sonnykh arterii" ("Thermographic methods and ultrasound Dopplerography in the follow-up of patients with lesioned carotid arteries"), Thesis for Candidate of Med. Sci. (Moscow: Central Research Laboratory, 1978)
57. Kolesov S N "Diagnosticheskie vozmozhnosti teplovideniya v neirokhirurgii" ("Diagnostic potential of thermovision in neurosurgery"), Thesis for Candidate of Med. Sci. (Moscow: Acad. N N Burdenko Institute of Neurosurgery of the Russ. Acad. of Medical Sci., 1980)
58. Pogosyan A M "Termografiya, ekhografiya i pritsel'naya aspiratsionnaya punktsiya v kompleksnoi diagnostike uzlovykh form zabolevanii shchitovidnoi zhelezy" ("Thermography, echography, and targeted aspiration biopsy in combined diagnosis of thyroid nodular disorders"), Thesis for Candidate of Med. Sci. (Moscow: Advanced Training Center for Doctors, 1980)
59. Voronov V G "Znachenie teplovizionnykh issledovanii v diagnostike opukholei spinnogo mozga" ("Role of thermovision studies in the diagnosis of spinal cord tumours"), Thesis for Candidate of Med. Sci. (Leningrad: A L Polenov Leningrad Research Neurosurgical Institute, 1985)
60. Krasnov D B "Diagnosticheskie vozmozhnosti funktsional'nogo teplovideniya pri povrezhdeniyakh nervov plecha i predplech'ya" ("Diagnostic potential of functional thermovision in patients with injured arm and forearm nerves"), Thesis for Candidate of Med. Sci. (Moscow: Acad. N N Burdenko Institute of Neurosurgery of the Russ. Acad. of Medical Sci., 1989)
61. Pavlov S A "Dinamika vosstanovleniya funktsii povrezhdennykh nervov konechnostei posle mikrokhirurgicheskogo vmeshatel'stva. Kliniko-eksperimental'noe issledovanie" ("Dynamics of functional restoration of lesioned nerves in the lower extremities after microneurosurgical intervention. Experimental investigation in clinic"), Thesis for Candidate of Med. Sci. (Moscow: Acad. N N Burdenko Institute of Neurosurgery of the Russ. Acad. of Medical Sci., 1989)
62. Fedosenko T S "Funktsional'noe teplovidenie i radiotermometriya v diagnostike radikulopatii u bol'nykh s osteokhondrozom poyasnichnogo otdela pozvonochnika" ("Functional thermovision and radiothermometry in the diagnosis of radiculopathies in patients with osteochondrosis of lumbar spine"), Thesis for Candidate of Med. Sci. (Nizhny Novgorod: Nizhny Novgorod State Medical Institute, 1993)
63. Popov V A "Kliniko-fiziologicheskaya kharakteristika teplovogo izlucheniya cheloveka v diagnostike i lechenii porazhenii krovenosnykh sosudov" ("Clinico-physiological characteristic of human thermal radiation in the diagnosis and management of lesioned blood vessels"), Thesis for Doctor of Med. Sci. (Arkhangel'sk: Arkhangel'sk State Medical Academy, 1997)
64. Nikitenko A I "Differentsial'naya diagnostika i khirurgicheskoe lechenie uzlovykh obrazovanii shchitovidnoi zhelezy" ("Differential diagnosis and surgical treatment of thyroid nodules"), Thesis for Candidate of Med. Sci. (Nizhny Novgorod: Nizhny Novgorod State Medical Academy, 1997)
65. Vlasov A L "Dinamicheskaya sverkhvysokochastotnaya radiotermografiya golovnogo mozga v norme i pri ishemicheskikh sostoyaniyakh" ("Dynamic microwave radiothermography of the brain in normal and ischemic states"), Thesis for Candidate of Med. Sci. (Perm': Acad. E A Vagner Perm' State Medical Academy, 2000)
66. Tolstova S S "Prognosticheskoe znachenie kombinirovannogo urodinamicheskogo issledovaniya pri termal'nykh metodakh lecheniya dobrokachestvennoi giperplazii prostaty" ("Prognostic value of combined urodynamic study in the treatment of benign prostatic hyperplasia by thermal methods"), Thesis for Candidate of Med. Sci. (Research Urology Institute of Ministry of Health of Russian Federation, 2001)
67. Khizhnyak L N "Diagnostika i kontrol' effektivnosti lecheniya zabolevanii sosudov niznikh konechnostei s ispol'zovaniem matrichnykh termovizionnykh sistem" ("Diagnosis and control of the efficiency of treatment of vascular lesions in lower limbs with the use of thermovision systems"), Thesis for Candidate of Med. Sci. (Tula: Tula State Univ., 2005)
68. Vail' Yu S, Varanovskii Ya M *Infrakrasnye Luchi v Klinicheskoi Diagnostike i Mediko-Biologicheskikh Issledovaniyakh* (Infrared Rays in Clinical Diagnostics and Biomedical Research) (Leningrad: Meditsina, 1969)
69. Vepkhvadze R Ya *Meditsinskaya Termografiya* (Medical Thermography) (Tbilisi: Sabchota Sakartvelo, 1975)
70. Zaretskii V V, Vykhovskaya A G *Klinicheskaya Termografiya* (Clinical Thermography) (Moscow: Meditsina, 1976)
71. Miroshnikov M M et al. *Teplovidenie i Ego Primenenie v Meditsine* (Thermovision and Its Medical Applications) (Moscow: Meditsina, 1981)
72. Likhterman L B *Ul'trazvukovaya Tomografiya i Teplovidenie v Neirokhirurgii* (Ultrasound Tomography and Thermovision in Neurosurgery) (Moscow: Meditsina, 1983)
73. Mazurin V Ya *Meditsinskaya Termografiya* (Medical Thermography) (Kishinev: Shtiintsa, 1984)
74. Stanier M W, Mount L E, Bligh J *Energy Balance and Temperature Regulation* (Cambridge Texts in the Physiological Sciences, Vol. 4) (Cambridge: Cambridge Univ. Press, 1984)
75. Karlov V A, Stulin I D, Bogin Yu N *Ul'trazvukovaya i Teplovizionnaya Diagnostika Sosudistykh Porazhenii Nervnoi Sistemy* (Ultrasound and Thermal Diagnosis of Vascular Lesions in the Nervous System) (Moscow: Meditsina, 1986)
76. Tikhonova A Ya *Sistema Termoregulyatsii pri Poyasnichnom Osteokhondroze* (Thermal Regulation System in Lumbar Osteochondrosis (Novosibirsk: Nauka, 1990)
77. Zenovko G I *Termografiya v Khirurgii* (Thermography in Surgery) (Moscow: Meditsina, 1998)

78. Miroshnikov M M et al. (Eds) *Teplovidenie v Gastroenterologii. Atlas Termogramm* (Thermovision in Gastroenterology. Atlas of Thermograms) (Moscow: Meditsina, 2000)
79. Anbar M *Quantitative Dynamic Telethermometry in Medical Diagnosis and Management* (Boca Raton: CRC Press, 1994)
80. Ivanitsky G R *Vestn. Ross. Akad. Nauk* **76** (1) 48 (2006) [Herald Russ. Acad. Sci. **76** 44 (2006)]
81. Anbar M, Haverly R F *Biomed. Thermology* **13** 173 (1994)
82. Anbar M et al. *Eur. J. Thermology* **7** 105 (1997)
83. Heller J S *West J. Med.* **142** 108 (1985)
84. Anbar M *Int. J. Technol. Assess. Health Care* **3** 613 (1987)
85. Anbar M *Cancer Lett.* **84** 23 (1994)
86. Igoshev I P et al. *Med. Radiol.* **30** (7) 63 (1985)
87. Gautherie M et al. *J. Microw. Power* **14** (2) 123 (1979)
88. Holthusen H, Arndt J O *J. Physiol.* (London) **487** 253 (1995)
89. Shetty V, Gratt B M, Flack V *J. Orofac. Pain* **8** 375 (1994)
90. Hejazi S, Anbar M *Biomed. Thermology* **10** 300 (1993)
91. Gratt B M, Sickles E A *J. Orofac. Pain* **9** 255 (1995)
92. Brock M, Risberg J, Ingvar D H *Brain Res.* **12** (l) 238 (1969)
93. Capistrant T D, Gumnit R J *Arch. Neurol.* **22** 499 (1970)
94. Capistrant T D, Gumnit R J *JAMA* **211** 656 (1970)
95. Capistrant T D, Gumnit R J *Neurology* **21** 427 (1971)
96. Enevoldsen E M, Jensen F T *J. Neurosurg.* **47** 699 (1977)
97. Green J *Orthopedics* **9** 1699 (1986)
98. Blaxter K "Energy exchange by radiation, convection, conduction, and evaporation", in *Energy Metabolism in Animals and Man* (New York: Cambridge Univ. Press, 1989) p. 86
99. Blaxter K "The minimal metabolism", in *Energy Metabolism in Animals and Man* (New York: Cambridge Univ. Press, 1989) p. 120
100. Gratt B M et al. *Dentomaxillofac Radiol.* **25** 247 (1996)
101. Grobklaus R, Bergmann K E "Physiology and regulation of body temperature", in *Thermological Methods* (Applied Thermology, Eds J-M Engel, U Flesch, and G Stüttgen) (Weinheim: VCH, 1985) p. 11
102. Krause B F *Nurse Anesth.* **4** (2) 55 (1993)
103. Chan F H et al. *Biomed. Mater. Eng.* **5** (3) 169 (1995)
104. Anbar M *Thermologie Österreich* **5** 15 (1995)
105. Granger D L, Miller W C, Hibbs J B "Methods in analyzing nitric oxide production in the immune response", in *Methods in Nitric Oxide Research* (Eds M Feelisch, J S Stamler) (Chichester: J. Wiley, 1996) p. 603
106. Hoffman R A, Langrehr J M, Simmons R L "The role of nitric oxide in allograft rejection", in *Nitric Oxide*: *Principles and Actions* (Ed. J Lancaster, Jr.) (San Diego: Academic Press, 1996) p. 237
107. Edrich J *J. Microw. Power* **14** (2) 95 (1979)
108. Palmer R M J et al. *Biochem. Biophys. Res. Commun.* **193** 398 (1993)
109. Biagioni P A et al. *Dentomaxillofac. Radiol.* **25** (3) 119 (1996)
110. Biagioni P A, McGimpsey J G, Lamey P J *Br. Dent. J.* **180** 226 (1996)
111. Canavan D, Gratt B M *Oral Surgery, Oral Med., Oral Pathol., Oral Radiol., Endodontology* **79** 778 (1995)
112. Chinzei T et al. *Biomed. Thermology* **15** 150 (1995)
113. Friedlander A H, Gratt B M *J. Oral Maxillofac. Surg.* **52** 1257 (1994)
114. Gratt B M et al. *J. Orofac. Pain* **8** 278 (1994)
115. Graff-Radford S B et al. *J. Orofac. Pain* **9** 138 (1995)
116. Gratt B M, Sickles E A, Shetty V *J. Orofac. Pain* **8** 369 (1994)
117. Gratt B M et al. *Oral Surgery, Oral Med., Oral Pathol., Oral Radiol., Endodontology* **80** 153 (1995)
118. Gratt B M et al. *J. Orofac. Pain* **8** 197 (1994)
119. Gratt B M, Sickles E A, Wexler C E *J. Orofac. Pain* **7** 345 (1993)
120. Steed P A *Cranio* **9** 120 (1991)
121. Anisimov A I et al. *Ortopediya, Travmatologiya i Protezirovanie* (1) 57 (1985)
122. Kolesov S N, Likhterman L B, Fraerman A P *Voprosy Neirokhirurgii* (1) 33 (1985)
123. Albert S H, Glickman M, Kallish M *Ann. N.Y. Acad. Sci.* **121** 157 (1964)
124. Backlund E O *J. Radiol. Electrol. Med. Nucl.* **48** (1) 39 (1967)
125. Baldy-Moulinier M et al. *Rev. Electroencephalogr. Neurophysiol. Clin.* **9** (2) 179 (1979)
126. McBeth S B, Gratt B M *Am. J. Orthodont. Dentofac. Orthoped.* **109** 481 (1996)
127. Beckman J S et al. *Biol. Chem. Hoppe-Seyler* **375** (2) 81 (1994)
128. Gratt B M, Sickles E A *J. Orofac. Pain* **7** 7 (1993)
129. Gulyaev Yu V, Godik E E, Dementienko V V *Dokl. Akad. Nauk SSSR* **299** 1259 (1988)
130. Podgul'ko K F, Tal'ko P A "Teplovidenie v kachestve metoda ob'ektivizatsii diagnostiki, effektivnosti lecheniya i ekspertizy netrudosposobnosti pri vertebrogennykh radikulitakh" ("Thermovision as a method for objectification of diagnosis, therapeutic efficiency, and assessment of disablement in patients with vertebrogenous radiculites"), in *Teplovidenie v Meditsine*. Tezisy Dokladov (Editor-in-Chief K S Ternovoi) (Kiev: 4-e Glavn. Upr. pri MZ UkrSSR, 1984) p. 41
131. Capistrant T D *Radiology* **100** (l) 85 (1971)
132. Benington I C et al. *J. Dentistry* **24** 263 (1996)
133. Ness R R, Ness B H "Thermography: its legal implications", in *Thermographic Evidence of Soft Tissue Injuries* (Ed. H Rein) (New York: McGraw-Hill, 1987) p. 8
134. Yanovskaya T B, Porokhova L N *Obratnye Zadachi Geofiziki* (Inverse Problems in Geophysics) 2nd ed. (St.-Petersburg: Izd. SPbGU, 2004)
135. Bilich G L (Ed.) *Bol'shoi Tolkovyi Meditsynskii Slovar'* (*Oxford*) (Large Defining Medical Dictionary) (Moscow: Veche. AST, 1998) p. 238; see also *Concise Medical Dictionary* 5th ed. (Oxford: Oxford Univ. Press, 1998)
136. Eroshevskii T I, Bochkareva A A (Eds) *Glaznye Bolezni* (Eye Diseases) (Moscow: Meditsina, 1977)
137. Ivanitsky G R et al. *Dokl. Ross. Akad. Nauk* **406** 840 (2006) [*Dokl. Biol. Sci.* **406** 22 (2006)]
138. Ivanitsky G R et al. *Dokl. Ross. Akad. Nauk* **393** 419 (2003) [*Dokl. Biol. Sci.* **393** 496 (2003)]
139. Ivanitsky G R et al. "Issledovanie mikrotsirkulyatsii krovi s pomoshch'yu sovremennykh metodov termografii pri vvedenii perftorana" ("Blood microcirculation studies by modern thermographic techniques during perftoran administration"), in *Perftoruglerodnye Soedineniya v Meditsine i Biologii* (Perfluorocarbon Compounds in Medicine and Biology) (Eds G R Ivanitsky, E B Zhiburt, E I Maevsky) (Pushchino, 2004) p. 10
140. Moroz V V et al. *Anesteziol. Reanimatol.* (6) 12 (1995)
141. Vorob'ev S I et al. "Sravnitel'noe izuchenie nekotorykh perftoruglerodnykh emul'sii" ("Comparative studies of certain perfluorocarbohydrate emulsions"), in *Fiziologicheskaya Aktivnost' Ftorsoderzhashchikh Soedinenii* (*Eksperiment i Klinika*) (Physiological Activity of Fluorine-Containing Compounds) (Experiment and Clinic) (Eds S I Vorob'ev, G R Ivanitsky) (Pushchino: PNTs RAN, 1995) p. 33
142. Maevsky E et al. *Artificial Cells, Blood Substitutes Biotechnol.* **33** 37 (2005)
143. Gervits L L et al. "Perfluoronated cycle-containing tertiary amines used as a basis for gas-conveying emulsions and device for the production thereof", Patent US 6,878,826 B2 (April 12, 2005) [*Biophysics* **46** 1 (2001)]
144. Ivanitsky G R *Biofizika* **46** 5 (2001) [*Biophysics* **46** 1 (2001)]
145. Maevsky E, Ivanitsky G "Oxygen-dependent and oxygen-independent effects of perftoran", in *Artificial Oxygen Carrier*: *Its Front Line* (Keio Univ. Intern. Symp. for Life Sciences and Medicine, Vol. 12, Eds K Kobayashi, E Tsuchida, H Horinouchi) (New York: Springer, 2004) p. 221
146. Ivanitsky G R, Maevsky E I *Biofizika* **49** 572 (2004) [*Biophysics* **49** 535 (2004)]